J. Fluid Mech. (2020), *vol.* 887, A20.
Published by Cambridge University Press
doi:10.1017/jfm.2019.1058

Marangoni instabilities associated with heated surfactant-laden falling films

S. J. D. D'Alessio[1,†], J. P. Pascal[2], E. Ellaban[2] and C. Ruyer-Quil[3]

[1]Faculty of Mathematics, University of Waterloo, Waterloo, Ontario, N2L 3G1, Canada

[2]Department of Mathematics, Ryerson University, Toronto, Ontario, M5B 2K3, Canada

[3]Université de Savoie Mont Blanc, CNRS, LOCIE 73000 Chambéry, France

(Received 10 June 2019; revised 4 October 2019; accepted 17 December 2019)

Investigated in this paper is the stability of the gravity-driven flow of a liquid layer laden with soluble surfactant down a heated incline. A mathematical model incorporating variations in surface tension with surfactant concentration and temperature has been formulated. A linear stability analysis is carried out both asymptotically for small wavenumbers and numerically for arbitrary wavenumbers. An expression for the critical Reynolds number has been derived which accounts for thermocapillary and solutocapillary effects, and reduces to known documented results for special cases. Also, a nonlinear reduced model has been derived using weighted residuals, and solved numerically to simulate the instability of the equilibrium flow and the development of permanent surface waves that arise. The nonlinear simulations were found to be in good agreement with the linear stability analysis.

Key words: thin films

1. Introduction

The Marangoni effect, named after the Italian physicist Carlo Marangoni, refers to mass transfer along the interface between two fluids arising from variations in surface tension. These variations are typically caused by gradients in solute/surfactant concentration, or temperature along the interface. When a concentration gradient is responsible for the variation in surface tension, the Marangoni effect is known as the solutocapillary effect, whereas when a temperature gradient drives the surface tension variation, then the Marangoni effect is referred to as the thermocapillary effect. In situations where both gradients are present, the solutocapillary and thermocapillary effects occur simultaneously. In this paper we study these competing effects by considering a thin liquid layer that is doped with a soluble surfactant and allowed to flow down an incline that is maintained at a higher temperature than that of the ambient surroundings. The initial experiments of Kapitza & Kapitza (1949) and the subsequent theoretical investigations of Benjamin (1957) and Yih (1963) have clearly demonstrated that an isothermal, surfactant-free, gravity-driven flow will become unstable provided that $Re > 5 \cot \beta/6$ where Re is the Reynolds number and β is

† Email address for correspondence: sdalessio@uwaterloo.ca

the inclination angle. While there have been numerous studies devoted to the impact on stability brought on by either the thermocapillary or solutocapillary effect acting alone, there have been relatively few studies focussing on the combined thermosolutal effects. This work attempts to partially fill this void.

The first studies to investigate thermocapillary effects resulting from thin-film flow over an inclined heated surface were carried out by Pearson (1958) and Sternling & Scriven (1959). These studies identified two thermocapillary instability modes: a short-wave mode and a long-wave mode. Goussis & Kelly (1991) later performed a detailed analysis into the onset of instability of a falling film down a uniformly heated wall. Comprehensive investigations into the long-wave instability were also conducted by Kalliadasis *et al.* (2003*a*), Kalliadasis, Kiyashko & Demekhin (2003*b*), Ruyer-Quil *et al.* (2005), Scheid *et al.* (2005) and Trevelyan *et al.* (2007). The key finding from these investigations is that in general thermocapillarity has a destabilizing effect on the flow. The work of D'Alessio *et al.* (2010) showed that this finding also holds for an uneven heated inclined surface; the only exception occurs in cases where strong surface tension is coupled with bottom unevenness. Here, thermocapillary effects can either stabilize or destabilize the flow depending on the Marangoni number and can also lead to a reversal in stability.

Introducing surfactants, which are chemical agents adsorbed by the surface, to a liquid layer typically has the effect of weakening surface tension (Aksel & Schörner 2018). However, contrary to thermocapillarity, solutocapillarity has a stabilizing influence on the flow. The first theoretical studies to uncover this stabilizing effect of surfactants in inclined flow were made by Benjamin (1964) and Whitaker (1964). They conducted a linear stability analysis on the governing equations for the case of an insoluble surfactant. Experimental validation of the stabilization accompanying the doping of a liquid layer with surfactants was reported by Emmert & Pigford (1954), Stirba & Hurt (1955) and Tailby & Portalski (1961), as well as with additional theoretical investigations carried out by Blyth & Pozrikidis (2004), Pereira *et al.* (2007),and Pereira & Kalliadasis (2008). To account for surfactant solubility Karapetsas & Bontozoglou (2013, 2014) have recently completed detailed studies on the stability. They found that surfactant solubility enhances flow instability and this finding has been experimentally verified by Georgantaki, Vlachogiannis & Bontozoglou (2016). Recently, Pascal, D'Alessio & Ellaban (2019) conducted an extension to include the effects of having a variable density.

Concerning the combined thermosolutal effects, one of the earliest studies was by Ji & Setterwall (1995). They considered film flow down a vertical wall which allowed for water vapour absorption along the free surface and identified three unstable modes. We note that Ji & Setterwall (1994) also numerically investigated the linear stability problem of soluble surfactants in a vertically falling film. They discovered that Marangoni effects destabilized the flow for moderate or short waves in the low-Reynolds-number range. Pascal & D'Alessio (2016) and D'Alessio & Pascal (2016) studied thermosolutal effects associated with inclined flow of a binary liquid with variable density. More recently Srivastava & Tiwari (2018) investigated gravity-driven film flow with an insoluble surfactant flowing down a vertical non-uniformly heated substrate. Using lubrication theory they derived evolution equations for the film thickness and surfactant concentration which were then used to elicit information regarding the impact on the stability of the flow.

The paper is structured as follows. In § 2 we present the governing equations and associated boundary conditions. Then in § 3 we carry out a linear stability analysis both asymptotically for small wavenumbers and numerically for arbitrary

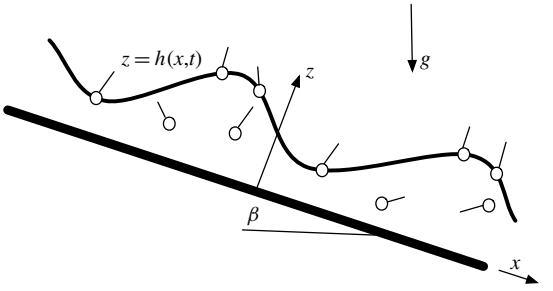

FIGURE 1. The flow set-up.

wavenumbers. Section 4 is devoted to studying nonlinear effects. A weighted residual model is derived and a numerical solution procedure is outlined. Finally, in § 5 we summarize the key findings of our investigation.

2. Mathematical formulation

Illustrated in figure 1 is a schematic of the problem under investigation. We are considering the two-dimensional gravity-driven flow of a thin liquid layer doped with a soluble surfactant down a heated incline making an angle β with the horizontal. The liquid is taken to be a viscous, incompressible, Newtonian fluid. The incline is maintained at a temperature T_0 while the constant ambient temperature is taken to be $T_a < T_0$. A rectangular coordinate system (x, z) has been adopted whereby the position of the free surface of the liquid layer corresponds to $z = h(x, t)$.

We assume that a fixed mass of surfactant is added to the liquid layer. Since we are dealing with a soluble surfactant, we must consider two separate concentrations: one for the surfactant adsorbed at the surface and another for the surfactant dissolved into the bulk of the layer. Further, we will assume that the surfactant concentrations are below the critical level for the formation of micelles, and thus, the surfactant added to the liquid will exist as monomers. Governing the conservation of surfactant mass in the bulk is the advection–diffusion equation given by

$$\frac{\partial c}{\partial t} + u\frac{\partial c}{\partial x} + w\frac{\partial c}{\partial z} = D_b\left(\frac{\partial^2 c}{\partial x^2} + \frac{\partial^2 c}{\partial z^2}\right),$$

where c is the concentration of surfactant dissolved in the bulk, D_b is the molecular diffusivity and (u, w) are the velocity components. In order to describe the transport of surfactant adsorbed at the surface we implement the following equation derived by Pereira & Kalliadasis (2011)

$$\frac{\partial \Gamma}{\partial t} + u\frac{\partial \Gamma}{\partial x} + \frac{\Gamma}{1+\left(\dfrac{\partial h}{\partial x}\right)^2}\left[\frac{\partial u}{\partial x} + \left(\frac{\partial h}{\partial x}\right)\left(\frac{\partial w}{\partial x}\right) + \frac{\partial h}{\partial x}\left(\frac{\partial u}{\partial z} + \frac{\partial h}{\partial x}\frac{\partial w}{\partial z}\right)\right]$$
$$= \frac{D_s}{\sqrt{1+\left(\dfrac{\partial h}{\partial x}\right)^2}}\frac{\partial}{\partial x}\left(\frac{\dfrac{\partial \Gamma}{\partial x}}{\sqrt{1+\left(\dfrac{\partial h}{\partial x}\right)^2}}\right) + J_{ba},$$

where $\Gamma(x, t)$ is the surface surfactant concentration, D_s is the surface molecular diffusivity and J_{ba} denotes the net flux of surfactant adsorbed at the surface. If we assume that the rate of adsorption is proportional to the concentration in the bulk, and that the rate of desorption is proportional to the surface concentration, then

$$J_{ba} = k_1 \left(1 - \frac{\Gamma}{\Gamma_\infty}\right) c - k_2 \Gamma \quad \text{at } z = h(x, t),$$

where k_1 and k_2 are the adsorption and desorption reaction rates, respectively, and Γ_∞ denotes the maximal packing surface concentration. Since the adsorption flux to the surface must also equal the surfactant flux from the bulk and since it is assumed to obey Fickian diffusion, J_{ba} can be expressed as

$$J_{ba} = \frac{D_b}{\sqrt{1 + \left(\dfrac{\partial h}{\partial x}\right)^2}} \left(\frac{\partial h}{\partial x}\frac{\partial c}{\partial x} - \frac{\partial c}{\partial z}\right) \quad \text{at } z = h(x, t).$$

Regarding the variation in surface tension, σ, we will allow it to vary linearly with both the surface surfactant concentration and the surface temperature as follows

$$\sigma(\Gamma, T) = \sigma_0 - \sigma_\Gamma(\Gamma - \Gamma_E) - \sigma_T(T - T_a),$$

where Γ_E is the equilibrium surface concentration and $\sigma_0 = \sigma(\Gamma_E, T_a)$. The parameters σ_Γ and σ_T are evaluated at $\Gamma = \Gamma_E$, $T = T_a$ and are defined by

$$\sigma_\Gamma = -\frac{\partial \sigma}{\partial \Gamma}, \quad \sigma_T = -\frac{\partial \sigma}{\partial T}.$$

They can be deduced from the equation of state for the surface tension for which there appear to be two commonly used expressions,

$$\sigma = \sigma_p[1 + \Gamma(\Sigma^{1/3} - 1)]^{-3}$$

known as the Sheludko (1967) equation, and

$$\sigma = \sigma_p + RT\Gamma_\infty \ln\left(1 - \frac{\Gamma}{\Gamma_\infty}\right)$$

known as the von Szyszkowski equation (Nepomnyashchy, Velarde & Colinet 2002).

Here, σ_p refers to the surface tension of a surfactant-free, or pure, liquid, R is the ideal gas constant, T is the temperature in Kelvin and Σ denotes the ratio of σ_p to the value corresponding to the maximal packing of surfactants. Since our interest is in the variation of surface tension with both surface surfactant concentration and surface temperature we will use the second expression; hence,

$$\sigma_\Gamma = \frac{RT_a\Gamma_\infty}{\Gamma_\infty - \Gamma_E} \quad \text{and} \quad \sigma_T = -R\Gamma_\infty \ln\left(1 - \frac{\Gamma_E}{\Gamma_\infty}\right).$$

We note that the von Szyszkowski equation becomes singular as $\Gamma \to \Gamma_\infty^-$. Since an underlying assumption is that the surfactant concentration remains below the critical level for the formation of micelles this singularity is of little consequence as Γ will be well below Γ_∞.

The conservation of mass, momentum and energy equations become (Spurk & Aksel 2008)

$$\frac{\partial u}{\partial x}+\frac{\partial w}{\partial z}=0,$$
$$\rho\left(\frac{\partial u}{\partial t}+u\frac{\partial u}{\partial x}+w\frac{\partial u}{\partial z}\right)=-\frac{\partial p}{\partial x}+\rho g\sin\beta+\mu\left(\frac{\partial^2 u}{\partial x^2}+\frac{\partial^2 u}{\partial z^2}\right),$$
$$\rho\left(\frac{\partial w}{\partial t}+u\frac{\partial w}{\partial x}+w\frac{\partial w}{\partial z}\right)=-\frac{\partial p}{\partial z}-\rho g\cos\beta+\mu\left(\frac{\partial^2 w}{\partial x^2}+\frac{\partial^2 w}{\partial z^2}\right),$$
$$\frac{\partial T}{\partial t}+u\frac{\partial T}{\partial x}+w\frac{\partial T}{\partial z}=\kappa\left(\frac{\partial^2 T}{\partial x^2}+\frac{\partial^2 T}{\partial z^2}\right),$$

where p is the pressure, g is the acceleration due to gravity, ρ is the density, μ is the dynamic viscosity and κ is the thermal diffusivity.

We next cast the governing equations in dimensionless form. In order to achieve this we choose the Nusselt thickness of a pure liquid given by

$$H=\left(\frac{3\mu Q}{g\rho\sin\beta}\right)^{1/3},$$

as a length scale. In the above Q denotes the prescribed flow rate. As for the surfactant concentration, there are two possible scales: Γ_∞ and Γ_E. We have decided to use the maximal value, Γ_∞. In the study conducted by Pereira & Kalliadasis (2008) they have opted to use Γ_E. For the pressure we use $\rho Q^2/H^2$ as the scale. Using these scales we apply the following transformation

$$(x,z)=H(x^*,z^*),\quad h=Hh^*,\quad t=\frac{H^2}{Q}t^*,\quad (u,w)=\frac{Q}{H}(u^*,w^*),$$
$$p-p_a=\frac{\rho Q^2}{H^2}p^*,\quad \Gamma=\Gamma_\infty\Gamma^*,\quad c=\frac{\Gamma_\infty}{H}c^*,$$

where p_a refers to the constant ambient pressure. Lastly, the temperature is scaled according to

$$T=T_a+(\Delta T)T^*,$$

where $\Delta T=T_0-T_a$.

With these scalings in place, and dropping the asterisks for notational convenience, the dimensionless equations within the liquid layer become

$$\frac{\partial u}{\partial x}+\frac{\partial w}{\partial z}=0, \tag{2.1}$$
$$Re\frac{\mathrm{D}u}{\mathrm{D}t}=-Re\frac{\partial p}{\partial x}+\frac{\partial^2 u}{\partial x^2}+\frac{\partial^2 u}{\partial z^2}+3, \tag{2.2}$$
$$Re\frac{\mathrm{D}w}{\mathrm{D}t}=-Re\frac{\partial p}{\partial z}+\frac{\partial^2 w}{\partial x^2}+\frac{\partial^2 w}{\partial z^2}-3\cot\beta, \tag{2.3}$$
$$Pe_b\frac{\mathrm{D}c}{\mathrm{D}t}=\frac{\partial^2 c}{\partial x^2}+\frac{\partial^2 c}{\partial z^2}, \tag{2.4}$$
$$PrRe\frac{\mathrm{D}T}{\mathrm{D}t}=\frac{\partial^2 T}{\partial x^2}+\frac{\partial^2 T}{\partial z^2}, \tag{2.5}$$

where $Pe_b = Q/D_b$ is the Péclet number, $Pr = \mu/\rho\kappa$ is the Prandtl number, $Re = \rho Q/\mu$ is the Reynolds number and $\mathrm{D}/\mathrm{D}t$ denotes the two-dimensional material derivative. Also, along the free surface the dimensionless equation for the surfactant transport takes the form

$$\frac{\partial \Gamma}{\partial t} + \frac{\partial \Gamma}{\partial x}u + \frac{\Gamma}{1+\left(\dfrac{\partial h}{\partial x}\right)^2}\left[\frac{\partial u}{\partial x} + \frac{\partial h}{\partial x}\frac{\partial w}{\partial x} + \frac{\partial h}{\partial x}\left(\frac{\partial u}{\partial z} + \frac{\partial h}{\partial x}\frac{\partial w}{\partial z}\right)\right]$$
$$= \frac{1}{Pe_s\sqrt{1+\left(\dfrac{\partial h}{\partial x}\right)^2}}\frac{\partial}{\partial x}\left(\frac{\dfrac{\partial \Gamma}{\partial x}}{\sqrt{1+\left(\dfrac{\partial h}{\partial x}\right)^2}}\right) + k_s[\xi_s(1-\Gamma)c - \Gamma] \quad \text{at } z = h(x,t), \tag{2.6}$$

where $Pe_s = Q/D_s$, $k_s = Hk_2/U$ and $\xi_s = k_1/k_2H$.

The system of equations (2.1)–(2.5) is to be solved subject to the following boundary conditions. Along the free surface $z = h(x, t)$ we impose the dynamic conditions

$$p = \frac{2}{Re\left(1+\left(\dfrac{\partial h}{\partial x}\right)^2\right)}\left[\frac{\partial u}{\partial x}\left(\left(\frac{\partial h}{\partial x}\right)^2 - 1\right) - \frac{\partial h}{\partial x}\left(\frac{\partial u}{\partial z} + \frac{\partial w}{\partial x}\right)\right]$$
$$- \frac{\dfrac{\partial^2 h}{\partial x^2}}{\left(1+\left(\dfrac{\partial h}{\partial x}\right)^2\right)^{3/2}}\left[We - M_1(\Gamma - \Gamma_E) - M_2 T\right], \tag{2.7}$$

$$-Re\sqrt{1+\left(\frac{\partial h}{\partial x}\right)^2}\left[M_1\frac{\partial \Gamma}{\partial x} + M_2\left(\frac{\partial T}{\partial x} + \frac{\partial h}{\partial x}\frac{\partial T}{\partial z}\right)\right]$$
$$= \left(1-\left(\frac{\partial h}{\partial x}\right)^2\right)\left(\frac{\partial w}{\partial x} + \frac{\partial u}{\partial z}\right) - 4\frac{\partial h}{\partial x}\frac{\partial u}{\partial x}, \tag{2.8}$$

$$\frac{1}{Pe_b\sqrt{1+\left(\dfrac{\partial h}{\partial x}\right)^2}}\left(\frac{\partial h}{\partial x}\frac{\partial c}{\partial x} - \frac{\partial c}{\partial z}\right) = k_s[\xi_s(1-\Gamma)c - \Gamma], \tag{2.9}$$

and

$$-BT\sqrt{1+\left(\frac{\partial h}{\partial x}\right)^2} = \frac{\partial T}{\partial z} - \frac{\partial h}{\partial x}\frac{\partial T}{\partial x}. \tag{2.10}$$

Conditions (2.7) and (2.8) arise from a balance between the ambient pressure and surface tension, condition (2.9) refers to balance between the surfactant adsorption flux and the diffusive flux from the bulk, while condition (2.10) is essentially a

statement of Newton's law of cooling. Here, $We = \sigma_0 H/\rho Q^2$, $M_1 = \sigma_\Gamma H\Gamma_\infty/\rho Q^2$, $M_2 = \sigma_T H\Delta T/\rho Q^2$ and $B = \alpha_g H/\rho c_p \kappa$ with α_g denoting the heat transfer coefficient across the liquid–air interface and c_p is the specific heat at constant pressure of the liquid. Ignoring evaporation the kinematic condition along the free surface is given by

$$w = \frac{\partial h}{\partial t} + u\frac{\partial h}{\partial x}, \quad \text{at } z = h(x,t). \tag{2.11}$$

Lastly, along the incline $z = 0$ we apply the no-slip, impermeability and constant temperature conditions

$$u = w = \frac{\partial c}{\partial z} = 0 \quad \text{and} \quad T = 1. \tag{2.12}$$

3. Linear stability analysis

In this section we will investigate the stability of a unidirectional steady flow which is constant in the streamwise direction. Setting all derivatives with respect to x and t to zero one easily obtains

$$\Gamma = \Gamma_E = \text{const.}, \quad c = c_E \equiv \frac{\Gamma_E}{\xi_s(1-\Gamma_E)}, \quad h = 1, \quad w = 0,$$
$$u = u_E(z) \equiv 3\left(z - \frac{z^2}{2}\right), \quad p = p_E(z) \equiv -\frac{3\cot\beta}{Re}(z-1), \quad T = T_E(z) \equiv 1 - \frac{Bz}{(1+B)},$$

where Γ_E assumes the role of a control parameter in the range $0 \leqslant \Gamma_E \leqslant 1$. Clearly, in order for c_E to remain bounded as $\Gamma_E \to 1^-$ it follows that we must also have $\xi_s \to \infty$ (i.e. an insoluble surfactant) such that the product $\xi_s(1-\Gamma_E)$ does not approach zero. More specifically, since we expect the surfactant concentration in the bulk to vanish in the insoluble limit, the product $\xi_s(1-\Gamma_E)$ must approach infinity. This suggests that a maximal surface concentration can only be attained if the surfactant is insoluble. Following Pascal *et al.* (2019) we will use $M_{tot} = \Gamma_E + c_E$ as a control parameter instead of Γ_E which are related by the following expression

$$\Gamma_E = \frac{1}{2}\left(1 + M_{tot} + \frac{1}{\xi_s} - \sqrt{(M_{tot}-1)^2 + \frac{2}{\xi_s}(M_{tot}+1) + \frac{1}{\xi_s^2}}\right). \tag{3.1}$$

The control parameters then become M_{tot}, ξ_s, k_s, β, Pe_b, Pe_s, Pr, B, M_1, M_2, We and Re.

To conduct a linear stability analysis we begin by disturbing the steady solution by adding an infinitesimal perturbation as follows

$$u = u_E + \tilde{u}, \quad w = \tilde{w}, \quad p = p_E + \tilde{p}, \quad h = 1 + \tilde{h},$$
$$\Gamma = \Gamma_E + \tilde{\Gamma}, \quad c = c_E + \tilde{c}, \quad T = T_E + \tilde{T},$$

where the tildes denote the perturbations. Next, we substitute these expressions into the governing equations and linearize with respect to the perturbations. To simplify the analysis we introduce the streamfunction, ψ, such that

$$\tilde{u} = \frac{\partial \psi}{\partial z}, \quad \tilde{w} = -\frac{\partial \psi}{\partial x}.$$

This guarantees that the continuity equation is automatically satisfied. We then eliminate the pressure perturbation by combining the momentum equations and employ normal modes given by

$$(\psi, \tilde{c}, \tilde{\Gamma}, \tilde{T}, \tilde{h}) = (\Psi(z), \hat{c}(z), \hat{\Gamma}, \hat{T}(z), \eta)\mathrm{e}^{\mathrm{i}k(x-vt)},$$

where the perturbation wavenumber, k, is taken to be real and positive, while v is a complex quantity with the real part denoting the phase speed and the imaginary part, $\mathrm{Im}(v)$, is related to the growth rate.

The functions $\Psi(z)$, $\hat{c}(z)$ and $\hat{T}(z)$ satisfy the following Orr–Sommerfeld type ordinary differential equations over the domain $0 < z < 1$

$$D^4\Psi - [\mathrm{i}kRe(u_E - v) + k^2]D^2\Psi + [-\mathrm{i}k^3Re(u_E - v) + k^4 + \mathrm{i}kReD^2u_E]\Psi = 0, \quad (3.2)$$

$$\mathrm{i}kPe_b(u_E - v)\hat{c} = D^2\hat{c} - k^2\hat{c}, \quad (3.3)$$

$$\mathrm{i}kPrRe(u_E - v)\hat{T} = D^2\hat{T} - k^2\hat{T} + \mathrm{i}kPe(DT_E)\Psi, \quad (3.4)$$

where $D \equiv \mathrm{d}/\mathrm{d}z$. The associated boundary conditions at $z = 1$ are

$$D^3\Psi - \left[\mathrm{i}kRe(u_E - v) + 2k^2\right]D\Psi - \left[3\mathrm{i}k\cot\beta + \mathrm{i}k^3(We - M_2T_E)\right]\eta = 0, \quad (3.5)$$

$$-\mathrm{i}kRe(M_1\hat{\Gamma} + M_2\hat{T}) = D^2\Psi + k^2\Psi - (3 - \mathrm{i}kReM_2DT_E)\eta, \quad (3.6)$$

$$\mathrm{i}k(u_E - v)\hat{\Gamma} + \mathrm{i}k\Gamma_E D\Psi = -\frac{k^2}{Pe_s}\hat{\Gamma} + k_s[\xi_s(1 - \Gamma_E)\hat{c} - (1 + \xi_s c_E)\hat{\Gamma}], \quad (3.7)$$

$$-D\hat{c} = Pe_b k_s[\xi_s(1 - \Gamma_E)\hat{c} - (1 + \xi_s c_E)\hat{\Gamma}], \quad (3.8)$$

$$D\hat{T} + B\hat{T} = -BDT_E\eta, \quad (3.9)$$

and

$$-\Psi = (u_E - v)\eta. \quad (3.10)$$

At $z = 0$ we have

$$\Psi = D\Psi = D\hat{c} = \hat{T} = 0. \quad (3.11)$$

The problem posed by (3.2)–(3.11) represents an eigenvalue problem with v denoting the eigenvalue which signals if the disturbance with wavenumber k will be amplified or damped in time for a given set of flow parameters. The system of (3.2)–(3.11) will be solved asymptotically as $k \to 0$ (i.e. longwave perturbations) and also numerically with no restriction on k.

3.1. *Asymptotic solution*

In carrying out the asymptotic analysis we begin by expanding the flow variables in powers of k as follows

$$\Psi = \Psi_0(z) + k\Psi_1(z) + \cdots,$$
$$\hat{c} = c_0(z) + kc_1(z) + \cdots,$$
$$\hat{T} = T_0(z) + kT_1(z) + \cdots,$$
$$\hat{\Gamma} = \Gamma_0 + k\Gamma_1 + \cdots,$$
$$\eta = \eta_0 + k\eta_1 + \cdots,$$
$$v = v_0 + kv_1 + \cdots$$

Without loss of generality we can normalize the eigenvalue problem and set $\eta_0 = 1$ and $\eta_1 = \eta_2 = 0$. An immediate consequence is that the perturbed free surface is given by $\tilde{h} = \mathrm{e}^{\mathrm{i}k(x-vt)}$. Substituting these expansions into the system (3.2)–(3.11), and assuming that all the parameters to be $O(1)$ as $k \to 0$, leads to a hierarchy of problems at various orders of k which can be solved sequentially.

The leading-order problem satisfies

$$D^4\Psi_0 = 0, \quad D^2 c_0 = 0, \quad D^2 T_0 = 0,$$

subject to the boundary conditions

$$\begin{gathered} D^3\Psi_0 = 0, \quad D^2\Psi_0 = 3, \quad v_0 = \Psi_0 - u_E, \quad Dc_0 = 0, \quad DT_0 + BT_0 = -BDT_E \quad \text{at } z = 1, \\ \xi_s(1-\Gamma_E)\phi_0 = (1+\xi_s\phi_E)\Gamma_0 \quad \text{at } z = 1, \\ Dc_0 = \Psi_0 = D\Psi_0 = 0 \quad \text{at } z = 0. \end{gathered}$$

The solutions are easily found to be

$$\Psi_0(z) = \frac{3}{2}z^2, \quad T_0(z) = \frac{B^2}{(1+B)^2}z, \quad \Gamma_0 = \frac{\xi_s(1-\Gamma_E)}{(1+\xi_s c_E)}c_0, \quad v_0 = 3,$$

where c_0 is a constant which is yet to be determined.

Proceeding to the $O(k)$ problem yields the system of equations

$$\begin{gathered} D^4\Psi_1 = \mathrm{i}Re(u_E - v_0)D^2\Psi_0 - \mathrm{i}ReD^2u_E\Psi_0, \\ D^2c_1 = \mathrm{i}Pe_b(u_E - v_0)c_0, \\ D^2T_1 = \mathrm{i}PrRe[(u_E - v_0)T_0 - DT_0\Psi_0], \end{gathered}$$

subject to

$$\begin{gathered} D^3\Psi_1 = \mathrm{i}Re(u_E - v_0)D\Psi_0 + 3\mathrm{i}\cot\beta \quad \text{at } z = 1, \\ D^2\Psi_1 = -\mathrm{i}Re(M_1\Gamma_0 + M_2T_0) - \mathrm{i}ReM_2DT_E \quad \text{at } z = 1, \\ \mathrm{D}c_1 = -\mathrm{i}Pe_b[(u_E - v_0)\Gamma_0 + \Gamma_E D\Psi_0] \quad \text{at } z = 1, \\ \mathrm{D}c_1 = -k_sPe_b[\xi_s(1-\Gamma_E)c_1 - (1+\xi_s c_E)\Gamma_1] \quad \text{at } z = 1, \\ \mathrm{D}T_1 + BT_1 = 0 \quad \text{at } z = 1, \\ \Psi_1 = v_1 \quad \text{at } z = 1, \\ \Psi_1 = D\Psi_1(0) = Dc_1 = T_1 = 0 \quad \text{at } z = 0. \end{gathered}$$

The condition for neutral stability can be obtained from v_1 given above in terms of Ψ_1. The solution for Ψ_1 was found to be

$$\Psi_1(z) = \frac{3\mathrm{i}Re}{40}(z^5 - 5z^4) + \frac{\mathrm{i}\cot\beta}{2}z^3 + \frac{\mathrm{i}Re}{2}\left[3\left(1 - \frac{\cot\beta}{Re}\right) - M_1\Gamma_0 + \frac{M_2B}{(1+B)^2}\right]z^2,$$

where

$$\Gamma_0 = \frac{6\Gamma_E\xi_s(1-\Gamma_E)^2}{4 + 3\xi_s(1-\Gamma_E)^2}.$$

Hence,

$$v_1 = \Psi_1(1) = \mathrm{i}Re\left(\frac{6}{5} - \frac{\cot\beta}{Re} + \frac{M_2B}{2(1+B)^2} - \frac{3M_1\Gamma_E\xi_s(1-\Gamma_E)^2}{4 + 3\xi_s(1-\Gamma_E)^2}\right),$$

with the state of neutral stability given by $v_1 = 0$. It is immediately evident that this relation is independent of the parameters Pr, Pe_s, Pe_b, We and k_s. Therefore the indication is that neutral stability is not affected by solutal and thermal diffusivity, nor is it influenced by the individual desorption and adsorption reaction rates, but only by the ratio of the two, which is given by the parameter ξ_s.

Now, the neutral stability relation can be written as the following expression for the critical Reynolds number, Re_{crit},

$$\frac{\cot\beta}{Re_{crit}} - \frac{6}{5} = F(B, \Gamma_E; M_1, M_2, \xi_s), \tag{3.12}$$

where

$$F(B, \Gamma_E; M_1, M_2, \xi_s) = \frac{M_2 B}{2(1+B)^2} - \frac{3M_1\Gamma_E\xi_s(1-\Gamma_E)^2}{4+3\xi_s(1-\Gamma_E)^2}.$$

For an isothermal clean liquid layer $F = 0$. The function F accounts for departures from $F = 0$, and hence variations in Re_{crit}, as a result of heating and doping, and is made up of two terms which clearly identify the contributions made by the thermal Marangoni effect and the soluto Marangoni effect, respectively. It is also clear that heating destabilizes the flow while the addition of a surfactant stabilizes the flow, as expected. We note that $F = 0$ can also occur when the thermosolutal mechanisms exactly cancel each other which happens when

$$\frac{M_2 B}{2(1+B)^2} = \frac{3M_1\Gamma_E\xi_s(1-\Gamma_E)^2}{4+3\xi_s(1-\Gamma_E)^2} \quad \text{or} \quad \frac{M_2}{M_1} = \frac{6\Gamma_E\xi_s(1+B)^2(1-\Gamma_E)^2}{B[4+3\xi_s(1-\Gamma_E)^2]}. \tag{3.13}$$

Thus, linear theory predicts the necessary relationship needed between the parameters in order for a heated liquid layer doped with a surfactant to have the same critical Reynolds number as the corresponding isothermal clean liquid layer.

To determine the extreme values of Re_{crit} over the semi-infinite rectangular strip $0 \leqslant B < \infty$, $0 \leqslant \Gamma_E \leqslant 1$ in the $B\Gamma_E$-plane we first find the critical points of F by solving

$$\frac{\partial F}{\partial B} = \frac{\partial F}{\partial \Gamma_E} = 0.$$

The critical points are found to be $(B, \Gamma_E) = (1, 1)$ or $(1, \overline{\Gamma}_E)$ where $\overline{\Gamma}_E$ is the real root of the cubic equation

$$3\xi_s\overline{\Gamma}_E^3 - 9\xi_s\overline{\Gamma}_E^2 + 9\xi_s\overline{\Gamma}_E + 12\overline{\Gamma}_E - 3\xi_s - 4 = 0,$$

given by

$$\overline{\Gamma}_E = 1 + \frac{a}{3\xi_s} - \frac{4}{a} \quad \text{where } a = \left(12\sqrt{3\xi_s^3(3\xi_s+4)} - 36\xi_s^2\right)^{1/3}.$$

It is worth noting that in the insoluble limit as $\xi_s \to \infty$, $\overline{\Gamma}_E \to 1^-$ and the two critical points merge. It turns out that the interior critical point $(B, \Gamma_E) = (1, \overline{\Gamma}_E)$ is a saddle point. Inspecting the values of F along the boundary we find that along $B = 0$ and $B \to \infty$ a minimum value of F is assumed given by

$$F_{min} = -\frac{3M_1\xi_s\overline{\Gamma}_E(1-\overline{\Gamma}_E)^2}{[4+3\xi_s(1-\overline{\Gamma}_E)^2]},$$

while along $\Gamma_E = 0$ and $\Gamma_E = 1$ a maximum value of F is assumed given by

$$F_{max} = \frac{M_2}{8}.$$

From this information the extreme values of Re_{crit} are

$$(Re_{crit})_{max} = \frac{5[4 + 3\xi_s(1 - \overline{\Gamma}_E)^2]\cot\beta}{3[8 + \xi_s(6 - 5\overline{\Gamma}_E M_1)(1 - \overline{\Gamma}_E)^2]} \quad \text{and} \quad (Re_{crit})_{min} = \frac{40\cot\beta}{48 + 5M_2}.$$

The existence of the saddle point $(B, \Gamma_E) = (1, \overline{\Gamma}_E)$ can be explained as follows. If we hold B constant at $B = 1$ and vary Γ_E we note that when $\Gamma_E = 0$ or $\Gamma_E = 1$ we obtain the above minimum value for Re_{crit}. Now, as we add a surfactant to an initially surfactant-free liquid layer gradients in the concentration will form along the free surface whereby the concentration is higher at the crests than at the troughs. This creates Marangoni stresses (i.e. solutocapillary forces) in the direction of the troughs which are responsible for damping surface deflections, and hence, stabilizing the flow. So a liquid layer with a non-uniform concentration of surface surfactant is more stable (i.e. has a larger Re_{crit} value) than a corresponding clean liquid layer because surfactants have a tendency of enhancing the elasticity of the surface. As more surfactant is added to the liquid layer the surface will eventually reach its maximal value. At this point the concentration gradients cannot form along the surface and consequently the liquid layer behaves exactly as a clean heated liquid layer. This is why $\Gamma_E = 0$ and $\Gamma_E = 1$ yield the same Re_{crit} value. Thus, there exists an optimal value of Γ_E, $\Gamma_E = \overline{\Gamma}_E$, that maximizes Re_{crit}. Similarly, if we fix the value of $\Gamma_E = \overline{\Gamma}_E$ and vary B we observe that when $B = 0$ or $B \to \infty$ we obtain the above maximum value for Re_{crit}. The case $B = 0$ corresponds to an insulated fluid layer which means that the temperature will be uniform throughout the layer. On the other hand, the case $B \to \infty$ corresponds to an infinite rate of heat transfer across the interface which means that the interface temperature will remain fixed at the ambient value. In both of these cases there is no temperature gradient along the free surface, and hence, no Marangoni stresses. Thus, the liquid layer will behave like an isothermal, surfactant-laden liquid layer. Now, as B increases from zero a temperature distribution in the liquid layer begins to develop and if the free surface is non-planar, then the temperature along the free surface will be greater at the troughs than at the crests. This temperature gradient creates Marangoni stresses (i.e. thermocapillary forces) which act to amplify the waves on the surface, and hence, destabilize the flow. However, for large B the temperature along the free surface will approach that of the ambient medium which is constant, and as such these thermocapillary forces will be weakened. Consequently, there exists a optimal value of B, $B = 1$, for which thermocapillarity is maximized resulting in a minimum value for Re_{crit}.

Alternatively, equation (3.12) can be written as

$$Re_{crit} = \frac{10(1 + B)^2[4 + 3\xi_s(1 - \Gamma_E)^2]\cot\beta}{6(1 + B)^2[8 + \xi_s(6 - 5\Gamma_E M_1)(1 - \Gamma_E)^2] + 5M_2 B[4 + 3\xi_s(1 - \Gamma_E)^2]}, \tag{3.14}$$

which can be expressed in terms of M_{tot} by making use of (3.1). There are various limits that can be taken and comparisons that can be drawn. For example, the isothermal limit can be obtained by setting $M_2 = 0$ or $B = 0$; this yields

$$Re_{crit}|_{B=0} = \frac{5[4 + 3\xi_s(1 - \Gamma_E)^2]\cot\beta}{3[8 + \xi_s(6 - 5\Gamma_E M_1)(1 - \Gamma_E)^2]}, \tag{3.15}$$

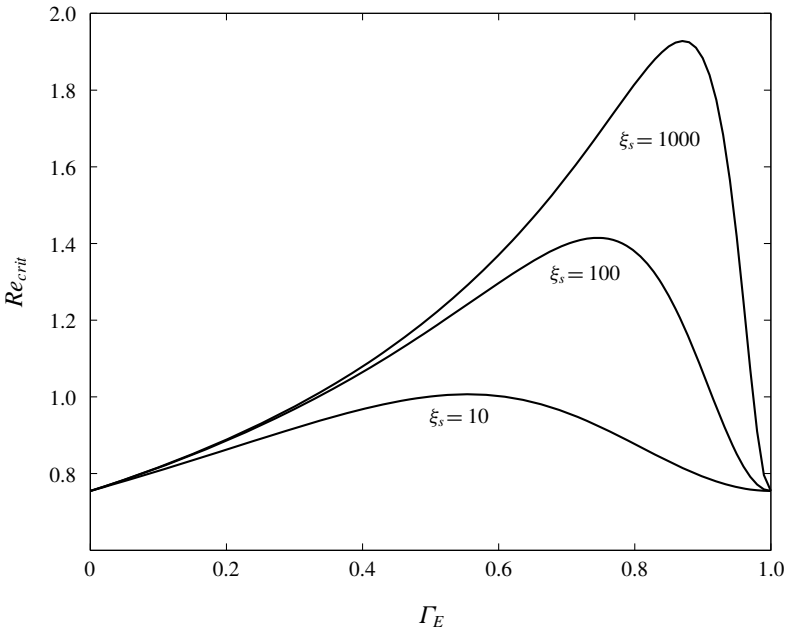

FIGURE 2. Value of Re_{crit} versus Γ_E for various values of ξ_s with $\cot\beta = M_1 = M_2 = B = 1$.

which coincides with the result obtained by Pascal *et al.* (2019) and also with Karapetsas & Bontozoglou (2014) if the difference in scaling is taken into account. The surfactant-free limit can be retrieved by setting $\Gamma_E = 0$ which gives

$$Re_{crit}|_{\Gamma_E=0} = \frac{10(1+B)^2\cot\beta}{12(1+B)^2 + 5M_2B}, \tag{3.16}$$

which is in full agreement with D'Alessio *et al.* (2010). Also, the insoluble case corresponds to the limit $\xi_s \to \infty$, $\Gamma_E \to 1^-$ such that $\xi_s(1-\Gamma_E)^2 \to 0$. This leads to

$$Re_{crit}|_{insoluble} = \frac{10(1+B)^2\cot\beta}{12(1+B)^2 + 5M_2B}, \tag{3.17}$$

which is identical to the surfactant-free limit. Plotted in figure 2 are curves of Re_{crit} as a function of Γ_E for various values of ξ_s. Lastly, expression (3.14) reproduces the familiar isothermal, surfactant-free case given by $Re_{crit} = 5\cot\beta/6$ when $B = \Gamma_E = 0$.

We next present a physical mechanism responsible for the stability of the flow as was done by Wei (2005) for the insoluble surfactant model and by Karapetsas & Bontozoglou (2014) for soluble surfactant case. We consider the flow rate given by

$$q = \int_0^1 (u_E + \tilde{u})\,\mathrm{d}z,$$

with $\tilde{u}(x, z, t) = \hat{u}(z)\tilde{h}(x, t)$. From the asymptotic analysis we find that

$$q = 1 + \frac{3}{2}\tilde{h} + \mathrm{i}kRe\tilde{h}\left(\frac{6}{5} - \frac{\cot\beta}{Re} + \frac{M_2B}{2(1+B)^2} - \frac{3M_1\Gamma_E\xi_s(1-\Gamma_E)^2}{4+3\xi_s(1-\Gamma_E)^2}\right) + O(k^2).$$

We recognize that the quantity in the brackets will be zero for neutral stability and thus changes sign as we cross from a stable (negative) to an unstable (positive) configuration. To leading order q and $\tilde{h}$ are in phase, but as we learned from the asymptotic analysis the $O(k)$ problem determines the stability. For non-neutral cases the first-order problem reveals a phase shift of $\pm\pi/2$ between q and $\tilde{h}$ where the sign corresponds to that of the quantity in the brackets. This phase shift is responsible for redistributing the fluid along the interface; when it is negative it has the effect of reducing the surface undulations and therefore stabilizes the flow, whereas when it is positive it causes fluid to pile up at the crest and in doing so destabilizes the flow. Now, the sign of the quantity in the brackets is influenced by the terms

$$\frac{M_2 B}{2(1+B)^2} \quad \text{and} \quad \frac{3M_1\Gamma_E\xi_s(1-\Gamma_E)^2}{4+3\xi_s(1-\Gamma_E)^2},$$

which have opposite signs, and these competing influences will contribute to the overall stability.

3.2. *Numerical solution*

In this investigation we are primarily interested in the H and S modes. Although there is also a shear mode, it has been shown by Floryan, Davis & Kelly (1987) that this mode will only be important at small inclination angles, and hence we will focus on moderate inclination angles. The scaling that we have adopted in § 2 allowed us to obtain a nice simple relation for neutral stability and to analyse the H mode in detail. However, in order to capture the S mode we need to introduce a second scaling because the parameters involved in the neutral stability relation are in fact implicitly dependent on the Reynolds number. Thus, a rescaling of the problem must be considered which involves strictly independent parameters in order to ensure that all physical aspects are fully and correctly taken into account. For example, in the standard non-isothermal case involving the stability of a heated clean fluid, it is well known that a Marangoni number independent of Re must be introduced in order for the analysis to resolve the separate mode of instability which is entirely driven by thermocapillarity and stabilized by inertia (Kalliadasis *et al.* 2012). The new non-dimensional numbers can be expressed in terms of the parameters currently appearing in the neutral stability relation as

$$M_1 = \left(\frac{3}{\sin\beta}\right)^{1/3}\frac{Ka\Sigma_1}{Re^{5/3}(1-\Gamma_E)}, \quad M_2 = -\left(\frac{3}{\sin\beta}\right)^{1/3}\frac{Ka\Sigma_2}{Re^{5/3}}\ln(1-\Gamma_E)$$
$$B = \left(\frac{3}{\sin\beta}\right)^{1/3} Re^{1/3}Bi, \quad \xi_s = \left(\frac{\sin\beta}{3}\right)^{1/3}\frac{\xi_a}{Re^{1/3}},$$

where the new parameters are the Kapitza number, given by $Ka = \sigma_p(\rho/\mu^4 g)^{1/3}$, the solutal and thermal capillarity parameters given by $\Sigma_1 = \Gamma_\infty RT_a/\sigma_p$ and $\Sigma_2 = \Gamma_\infty R\Delta T/\sigma_p$, respectively, the rate of adsorption parameter $\xi_a = (g\rho^2/\mu^2)^{1/3}k_1/k_2$ and the Biot number $Bi = \alpha_g/\rho c_p\kappa(\mu/\rho)^{2/3}g^{-1/3}$. Here, we have also incorporated the von Szyszkowski equation of state. We point out that in terms of these new parameters the neutral stability relation cannot be explicitly solved for the Reynolds number and the role played by the various physical factors cannot be clearly identified with separate terms as was done in (3.12). Shortly we will use this new relation to

generate and interpret plots of neutral stability curves, but listing the formulation serves little purpose. Lastly, we must entertain the possibility that infinitely long perturbations are not the most unstable, in which case the neutral stability relation obtained from the asymptotic analysis does not accurately predict the threshold of instability for the equilibrium flow.

In order to determine the stability of perturbations of arbitrary wavenumber we employed a collocation method based on polynomial interpolation with Chebyshev points (Trefethen 2000) to solve the eigenvalue problem (3.2)–(3.11). Accordingly, we introduced the expansions

$$\Psi = \sum_{j=0}^{N} w_j P_j(\xi), \quad \hat{c} = \sum_{j=0}^{N} v_j P_j(\xi), \quad \hat{T} = \sum_{j=0}^{N} \zeta_j P_j(\xi),$$

where $\xi = 2z - 1$ and

$$P_j(\xi) = \frac{\displaystyle\prod_{\substack{n=0 \\ n\neq j}}^{N} (\xi - \xi_n)}{\displaystyle\prod_{\substack{n=0 \\ n\neq j}}^{N} (\xi_j - \xi_n)}, \quad j = 0, 1, 2, \ldots, N,$$

with $\xi_l = -\cos(l\pi/N)$, $l = 0,\ 1,\ 2, \ldots,\ N$. This leads to an algebraic system of the form

$$\boldsymbol{\mathcal{A}} y = v \boldsymbol{\mathcal{B}} y,$$

where

$$y = [w_0\, w_1\ \cdots\ w_N\, v_0\, v_1\ \cdots\ v_N\, \zeta_0\, \zeta_1\ \cdots\ \zeta_N\, \eta\ \hat{\Gamma}]^T,$$

and $\boldsymbol{\mathcal{A}}$ and $\boldsymbol{\mathcal{B}}$ are $(3N + 5) \times (3N + 5)$ matrices. The eigenvalues of this system were calculated using the Matlab subroutine `eig`. The correct eigenvalue for the problem (3.2)–(3.11) was determined by recalculating the eigenvalues of the algebraic system for a finer grid and identifying the value that remained unchanged. The results from the collocation method confirm that the onset of instability in the equilibrium flow is in fact due to the amplification of infinitely long perturbations, and the critical conditions for instability are in excellent agreement with the predictions from the asymptotic analysis, as is illustrated in figure 3. This is similar to what is known to be the case for both isothermal flow with surfactants (Pascal *et al.* 2019) and a clean fluid in a non-isothermal flow (Ellaban, Pascal & D'Alessio 2017).

In presenting and interpreting our results we examine the stability map in the $\Sigma_2 Re$-plane. We plot the curves which denote the values of Re and Σ_2 associated with neutral stability for the equilibrium flow. The region to the right of the neutral stability curve corresponds to instability, while for Re and Σ_2 combinations in the region to the left the equilibrium flow is stable. As Σ_2 is the parameter measuring thermocapillarity, this observation is consistent with the destabilizing role played by the thermal Marangoni effect. There is also a critical level of thermocapillarity beyond which the flow is unstable for all Reynolds number. This is identified by the maximum Σ_2 value on the neutral stability curve. For lower values the flow is stable depending on the Reynolds number. For the basic non-isothermal flow of a clean fluid two separate modes of instability are known to exist: the so-called H mode which

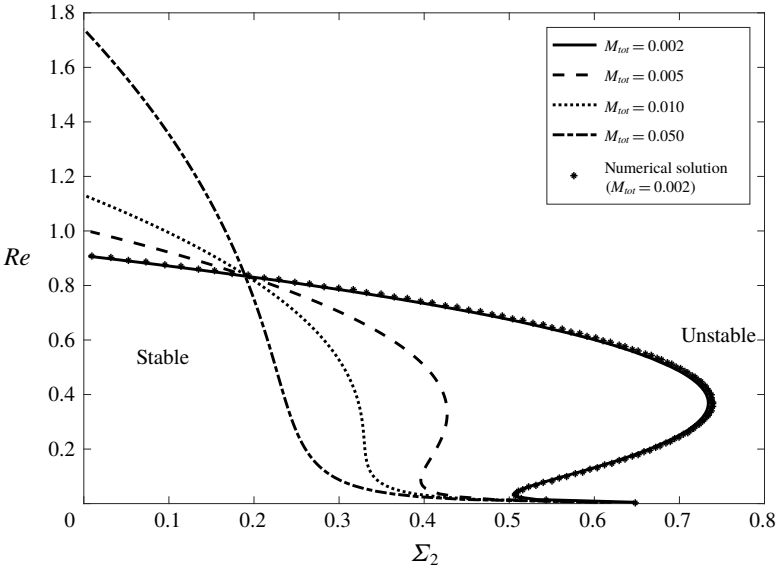

FIGURE 3. Neutral stability curves for different values of M_{tot} in the $\Sigma_2 Re$-plane with $\Sigma_1 = 0.07$, $\xi_a = 1$, $Ka = 3000$ and $Bi = 1$.

is driven by inertia and enhanced by thermocapillarity, hence distinguishable by the stability occurring as the Reynolds number is increased beyond a critical value, and the so-called S mode which is driven by thermocapillarity and impeded by inertia and occurring as the Reynolds number is decreased below a critical level.

In figure 3 we plot the neutral stability curves for different values of M_{tot} which measures the total concentration of surfactant added to the equilibrium flow. For one of the cases presented we also compare the numerical solution with that obtained by our asymptotic analysis and we see that the agreement is excellent. For small Σ_2 values (i.e. weak thermocapillarity) only the H mode is present. This is indicated by the fact that instability results as the Reynolds number is increased beyond the value for neutral stability, and it can be seen that the critical Reynolds number increases with M_{tot}. This behaviour is identical to isothermal flow for sufficiently low surfactant concentration, when adding a surfactant stabilizes the flow, as was explained above. However, for sufficiently large values of Σ_2 the region of stability shrinks as M_{tot} is increased, meaning that adding more surfactant destabilizes the flow. As such, thermocapillarity effectuates a reversal in the stabilizing effect of surfactant doping. Now, the formula in (3.12) consists of separate terms for the solutal and thermal contributions to Re_{crit}, and therefore does not capture this coupling of the two effects. The explanation is the fact that the formula is in terms of the original parameters which are implicitly dependent on Re_{crit}, and it is thus evident that it is important to introduce the new parameters in order to accurately interpret the results.

Continuing with our examination of the results in figure 3 we see that for the smaller values of M_{tot}, the curves clearly display the occurrence of both modes of instability for sufficiently large values of Σ_2. Specifically, for low Reynolds numbers the flow is unstable due to the S mode and for sufficiently high Reynolds numbers the H mode destabilizes the flow. The thresholds for the two modes are marked by two critical Re values located on the neutral stability curve, with the interval

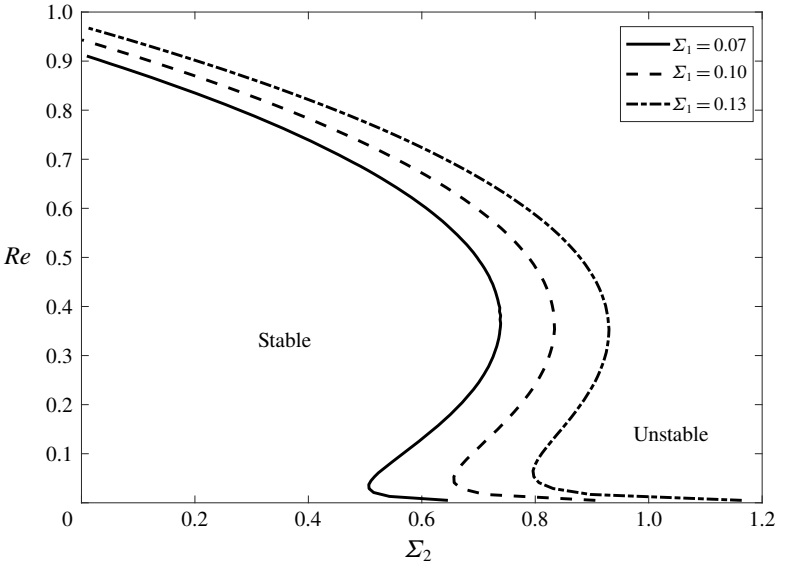

FIGURE 4. Neutral stability curves for different values of Σ_1 in the $\Sigma_2 Re$-plane with $\xi_a = 1$, $M_{tot} = 0.002$, $Ka = 3000$ and $Bi = 1$.

between them corresponding to Reynolds numbers for which the flow is stable. It is interesting to note that adding surfactant stabilizes the flow for a narrow interval of small Reynolds numbers. Although the physical explanation for this is not clear, it is predicted by both our numerical and asymptotic results. As M_{tot} is increased the S mode eventually disappears due to the rapid destabilization of the H mode which is triggered at significantly reduced levels of inertia. However, the thin region of stability next to the $Re = 0$ axis persists and its extent with respect to Σ_2 values remains approximately fixed.

In the next set of results illustrated in figure 4 we show the effect of the parameter Σ_1, which is related to the rate of variation in surface tension with respect to surfactant concentration. In determining a realistic range of values for this parameter we assumed that the value of the maximal surface concentration is $\Gamma_\infty = 2 \times 10^{-6}$ mol m^{-2}, as was done by Pereira & Kalliadasis (2008). Then with $R = 8.3145$ N m mol^{-1} K^{-1} and $T_a = 25\,^\circ$C $= 298.15$ K, and using $\sigma_p = 72 \times 10^{-3}$ N m^{-1} (the surface tension of water at 25 °C) we obtain $\Sigma_1 \approx 0.07$. It can be clearly seen that the region of stability increases with Σ_1 due to the stabilization of both the H and S modes. Since the rate of variation of surface tension with surfactant concentration is proportional to Σ_1, increasing this parameter strengthens the solutocapillary stresses which damp surface perturbations thus stabilizing the inertia-driven H mode. The fact that the S mode is stabilized indicates that solutocapillarity also counteracts the instability driven entirely by thermocapillarity.

Finally, in figure 5 we present the neutral stability curves for different values of ξ_a. It is apparent that the region of stability increases with ξ_a, meaning that increasing surfactant solubility, which is associated with a decrease in ξ_a, destabilizes the flow regardless of the level of thermocapillarity. This behaviour is consistent with the fact that desorption of surfactant from the surface lowers concentration gradients along the surface and weakens the solutal Marangoni stresses.

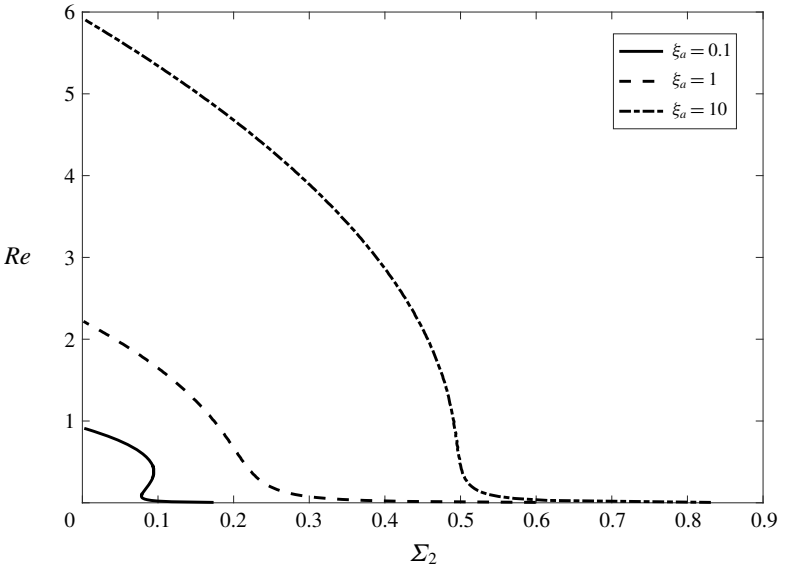

FIGURE 5. Neutral stability curves for different values of ξ_a in the $\Sigma_2 Re$-plane with $\Sigma_1 = 0.07$, $M_{tot} = 0.1$, $Ka = 3000$ and $Bi = 1$.

To complete our linear stability analysis we now consider the stability of different perturbation wavenumbers. This can be gauged from the results in figure 6 where we present the neutral stability curves in the Rek-plane for different values of Σ_2 with $M_{tot} = 0.005$, calculated using the numerical method. We first note that these results confirm that perturbations with $k = 0$ are the most unstable as claimed above. Specifically, we see that the intervals of stable Reynolds numbers are narrowest for $k = 0$ and widen as k is increased. The intercepts of the curves with the Re axis coincide with the critical Reynolds numbers for the onset of instability in the equilibrium flow at the specified Σ_2 values on the curve in figure 3 for $M_{tot} = 0.005$. We also observe the merging of the H and S modes for $\Sigma_2 = 0.42713$. Also apparent in these results is that the shape of the S-mode branch of the curve is different from the one known to be obtained for a clean fluid. In that case k decreases monotonically with Re (Kalliadasis *et al.* 2012), while here it attains a maximum. In other words, for the basic non-isothermal flow, as Re is decreased and inertia is lowered, more wavenumbers are destabilized by thermocapillarity. However, if surfactant is added a stabilizing effect takes place for very low Reynolds numbers and the range of unstable wavenumbers is reduced as Re is decreased. Eventually all wavenumbers are stabilized resulting in a stable flow.

4. Nonlinear simulations

In this section we investigate the effect of nonlinearity on the stability of the flow. Since the S mode occurs at small Reynolds numbers and the weighted residual approximation is better suited to resolve the H mode at larger Reynolds numbers we revert back to the original scaling applied in § 2. We begin by introducing slow time (τ) and space (X) variables and rescale the vertical velocity (W) according to

$$\tau = \varepsilon t, \quad X = \varepsilon x, \quad w = \varepsilon W,$$

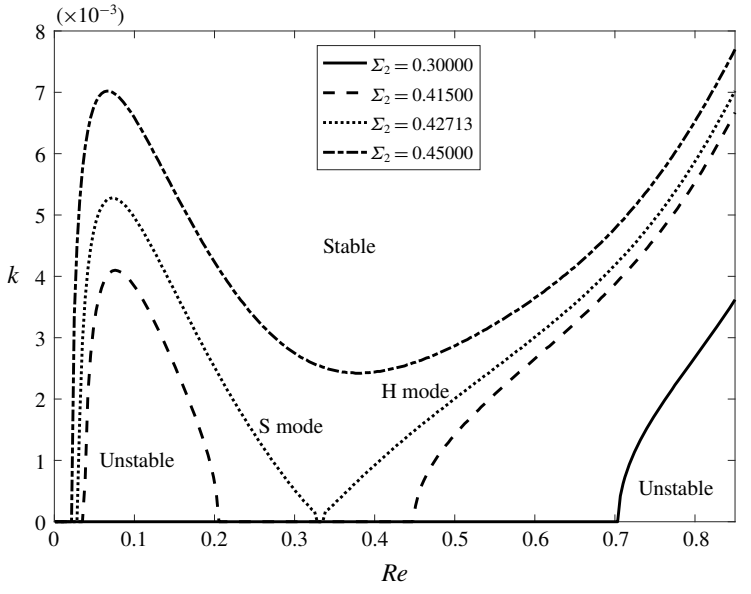

FIGURE 6. Neutral stability curves for different values of Σ_2 in the Rek-plane with $M_{tot} = 0.005$, $\Sigma_1 = 0.07$, $\xi_a = 1$, $Ka = 3000$, $Bi = 1$, $Pr = 7$, $Sc_b = Sc_s = 700$ and $k_d = 1$, where $Sc_b = \mu/\rho D_b$, $Sc_s = \mu/\rho D_s$ and $k_d = (\mu/g^2\rho)^{1/3}k_2$.

where $0 < \varepsilon \ll 1$ is a small parameter. Then the scaled governing equations (2.1)–(2.5) to second order in ε become

$$\frac{\partial u}{\partial X} + \frac{\partial W}{\partial z} = 0, \tag{4.1}$$

$$\varepsilon Re\left(\frac{\partial u}{\partial \tau} + u\frac{\partial u}{\partial X} + W\frac{\partial u}{\partial z}\right) = -\varepsilon Re\frac{\partial p}{\partial X} + 3 + \varepsilon^2\frac{\partial^2 u}{\partial X^2} + \frac{\partial^2 u}{\partial z^2}, \tag{4.2}$$

$$\varepsilon^2 Re\left(\frac{\partial W}{\partial \tau} + u\frac{\partial W}{\partial X} + W\frac{\partial W}{\partial z}\right) = -Re\frac{\partial p}{\partial z} - 3\cot\beta + \varepsilon\frac{\partial^2 W}{\partial z^2}, \tag{4.3}$$

$$\varepsilon Pe_b\left(\frac{\partial c}{\partial \tau} + u\frac{\partial c}{\partial X} + W\frac{\partial c}{\partial z}\right) = \varepsilon^2\frac{\partial^2 c}{\partial X^2} + \frac{\partial^2 c}{\partial z^2}, \tag{4.4}$$

$$\varepsilon PrRe\left(\frac{\partial T}{\partial \tau} + u\frac{\partial T}{\partial X} + W\frac{\partial T}{\partial z}\right) = \varepsilon^2\frac{\partial^2 T}{\partial X^2} + \frac{\partial^2 T}{\partial z^2}. \tag{4.5}$$

These can be viewed as the long-wave equations and mark the starting point of our nonlinear analysis.

Likewise, the transformed boundary conditions at $z = h(X, \tau)$ to second order in ε are

$$p = \frac{2\varepsilon}{Re}\left(\frac{\partial W}{\partial z} - \frac{\partial h}{\partial X}\frac{\partial u}{\partial z}\right) - \varepsilon^2\left[We - M_1(\Gamma - \Gamma_E) - M_2 T\right]\frac{\partial^2 h}{\partial X^2}, \tag{4.6}$$

$$W = \frac{\partial h}{\partial \tau} + u\frac{\partial h}{\partial X}, \tag{4.7}$$

$$\varepsilon\left(\frac{\partial \Gamma}{\partial \tau} + u\frac{\partial \Gamma}{\partial X}\right) + \varepsilon\Gamma\left(\frac{\partial u}{\partial X} + \frac{\partial h}{\partial X}\frac{\partial u}{\partial z}\right) = \frac{\varepsilon^2}{Pe_s}\frac{\partial^2 \Gamma}{\partial X^2} + k_s\left[\xi_s(1-\Gamma)c - \Gamma\right], \tag{4.8}$$

$$\varepsilon^2 \frac{\partial h}{\partial X}\frac{\partial c}{\partial X} - \frac{\partial c}{\partial z} = Pe_b k_s \left[\xi_s(1-\Gamma)c - \Gamma\right], \tag{4.9}$$

$$-\varepsilon Re \left[M_1 \frac{\partial \Gamma}{\partial X} + M_2 \left(\frac{\partial T}{\partial X} + \frac{\partial h}{\partial X}\frac{\partial T}{\partial z}\right)\right] = \frac{\partial u}{\partial z} + \varepsilon^2 \frac{\partial W}{\partial X} - 4\varepsilon^2 \frac{\partial h}{\partial X}\frac{\partial u}{\partial X}, \tag{4.10}$$

$$-BT = \frac{\partial T}{\partial z} - \varepsilon^2 \frac{\partial h}{\partial X}\frac{\partial T}{\partial X}, \tag{4.11}$$

while the bottom conditions at $z = 0$ are

$$u = W = \frac{\partial c}{\partial z} = 0, \quad T = 1. \tag{4.12}$$

4.1. *Weighted residual model*

We next implement a reduced model where the explicit dependence on the vertical coordinate is eliminated by applying a weighted residual technique. The method of weighted residuals was originally proposed by Ruyer-Quil & Manneville (2000, 2002) to handle isothermal flows down an even incline. It has since been applied to more complicated flows (Kalliadasis *et al.* 2003*a*; D'Alessio, Pascal & Jasmine 2009; Pascal & D'Alessio 2010; D'Alessio *et al.* 2010; Ogden, D'Alessio & Pascal 2011; Pascal & D'Alessio 2016; D'Alessio & Pascal 2016; Ellaban *et al.* 2017; Pascal, D'Alessio & Hasan 2018). Recently, Veremieiev & Wacks (2019) have extended the weighted residual method to include third- and fourth-order terms. Here, we extend the approach implemented by Pascal *et al.* (2019) to incorporate thermosoluto effects.

The basic idea behind the weighted residual method is to eliminate the z dependence by prescribing specific profiles for u, T and c. We propose the following:

$$u = \frac{3q}{2h^3} b + \frac{\varepsilon Re}{4h}\left(M_1 \frac{\partial \Gamma}{\partial X} + M_2 \frac{\partial \theta}{\partial X}\right) b_1,$$

$$T = 1 + \frac{(\theta - 1)}{h} z,$$

$$c = C + \frac{Pe_b k_s}{2h}\left[\xi_s(1-\Gamma)C - \Gamma\right](h^2 - z^2),$$

where b and b_1 are given by

$$b = z(2h - z), \quad b_1 = z(2h - 3z).$$

We note that the proposed profile for T represents a linear variation in temperature with respect to z, while that for c corresponds to a linear variation in the gradient $\partial c/\partial z$ with respect to z. Here, $C(X, \tau) = c(X, z = h, \tau)$ denotes the bulk concentration at the interface, whereas $\theta(X, \tau) = T(X, z = h, \tau)$ is the surface temperature, and

$$q = \int_0^h u \, \mathrm{d}z,$$

is the flow rate. We point out that the profiles for u and c satisfy all the boundary conditions including the free-surface conditions to $O(\varepsilon^2)$. Although the profile for T satisfies the bottom condition, it does not satisfy the free-surface condition. In fact, it is impossible for the profile to satisfy both. However, as explained by

Kalliadasis *et al.* (2003*a*), the free-surface condition is incorporated into the energy equation when it is integrated over the fluid thickness, as described below. The profiles for u and T have been used in previous studies, whereas the particular choice for c is new and an explanation behind this choice is given in appendix A.

In accordance with the Galerkin approach we take b as the weight function and multiply (4.2) by b and integrate with respect to z from 0 to h. The pressure term in (4.2) is eliminated by using (4.3) as follows. First, we discard the $O(\varepsilon^2)$ terms to obtain

$$\frac{\partial p}{\partial z} = -\frac{3\cot\beta}{Re} + \frac{\varepsilon}{Re}\frac{\partial^2 W}{\partial z^2}.$$

This is then integrated from z to h and the boundary condition (4.6) at $z=h$ is applied to yield an expression for the pressure which is then substituted into (4.2). Since the pressure term is multiplied by ε in (4.2), the $O(\varepsilon^2)$ terms in (4.3) can be ignored. This will result in a second-order weighted residual model. For the concentration equation we take the weight function to be unity and integrate from $z=0$ to $z=h$, while for the energy equation we choose z as the weight function and integrate over the liquid layer. After some algebra we obtain the following second-order equations for the flow variables h, q, $\phi = h(\theta-1)$, $\chi = h^2[\xi_s(1-\Gamma)C-\Gamma]$ and Γ

$$\frac{\partial h}{\partial \tau} + \frac{\partial q}{\partial X} = 0, \tag{4.13}$$

$$\begin{aligned}\frac{\partial q}{\partial \tau} + \frac{\partial}{\partial X}\left[\frac{9}{7}\frac{q^2}{h} + \frac{5\cot\beta}{4Re}h^2 + \frac{5M_1}{4}\Gamma + \frac{5M_2}{4}\frac{\phi}{h}\right] &= \frac{q}{7h}\frac{\partial q}{\partial X} + \frac{5}{2\varepsilon Re}\left(h - \frac{q}{h^2}\right)\\ &+ \frac{\varepsilon}{Re}\left[\frac{9}{2}\frac{\partial^2 q}{\partial X^2} - \frac{9}{2h}\frac{\partial h}{\partial X}\frac{\partial q}{\partial X} + \frac{4q}{h^2}\left(\frac{\partial h}{\partial X}\right)^2 - \frac{6q}{h}\frac{\partial^2 h}{\partial X^2}\right]\\ &+ \frac{\varepsilon M_1 Re}{16}\left[\frac{h^2}{3}\frac{\partial^2\Gamma}{\partial X\partial\tau} + \frac{15hq}{14}\frac{\partial^2\Gamma}{\partial X^2} + \frac{19h}{21}\frac{\partial\Gamma}{\partial X}\frac{\partial q}{\partial X} + \frac{5q}{7}\frac{\partial h}{\partial X}\frac{\partial\Gamma}{\partial X}\right]\\ &+ \frac{\varepsilon M_2 Re}{16}\left[\frac{h}{3}\frac{\partial^2\phi}{\partial X\partial\tau} - \frac{1}{3}\frac{\partial h}{\partial X}\frac{\partial\phi}{\partial\tau} + \frac{26}{21}\frac{\partial\phi}{\partial X}\frac{\partial q}{\partial X} - \frac{11\phi}{7h}\frac{\partial h}{\partial X}\frac{\partial q}{\partial X} + \frac{\phi}{3}\frac{\partial^2 q}{\partial X^2}\right.\\ &\left.+ \frac{15q}{14}\frac{\partial^2\phi}{\partial X^2} - \frac{10q}{7h}\frac{\partial h}{\partial X}\frac{\partial\phi}{\partial X} + \frac{10q\phi}{7h^2}\left(\frac{\partial h}{\partial X}\right)^2 - \frac{15q\phi}{14h}\frac{\partial^2 h}{\partial X^2}\right],\end{aligned} \tag{4.14}$$

$$\begin{aligned}\frac{\partial\phi}{\partial\tau} + \frac{\partial}{\partial X}\left[\frac{27}{20}\frac{q\phi}{h}\right] &= \frac{7\phi}{40h}\frac{\partial q}{\partial X} - \frac{3}{\varepsilon PrReh}\left[B(h+\phi) + \frac{\phi}{h}\right]\\ &+ \frac{3\varepsilon M_1 Re}{80}\left[h\phi\frac{\partial^2\Gamma}{\partial X^2} + 2h\frac{\partial\phi}{\partial X}\frac{\partial\Gamma}{\partial X}\right]\\ &+ \frac{\varepsilon}{PrRe}\left[\frac{\partial^2\phi}{\partial X^2} - \frac{1}{h}\frac{\partial h}{\partial X}\frac{\partial\phi}{\partial X} - \frac{2\phi}{h}\frac{\partial^2 h}{\partial X^2} - \frac{3B}{2}\left(1+\frac{\phi}{h}\right)\left(\frac{\partial h}{\partial X}\right)^2\right]\\ &+ \frac{3\varepsilon M_2 Re}{80}\left[\phi\frac{\partial^2\phi}{\partial X^2} + 2\left(\frac{\partial\phi}{\partial X}\right)^2 - \frac{4\phi}{h}\frac{\partial h}{\partial X}\frac{\partial\phi}{\partial X} - \frac{\phi^2}{h}\frac{\partial^2 h}{\partial X^2} + \frac{2\phi^2}{h^2}\left(\frac{\partial h}{\partial X}\right)^2\right],\end{aligned} \tag{4.15}$$

$$\frac{\partial}{\partial\tau}\left(\chi+\frac{3hC}{Pe_bk_s}\right)+\frac{\partial}{\partial X}\left[\frac{33}{40}\frac{q\chi}{h}+\frac{3qC}{Pe_bk_s}\right]$$
$$=\frac{\varepsilon}{Pe_b}\left[\frac{\partial^2\chi}{\partial X^2}-\frac{3\chi}{h^2}\left(\frac{\partial h}{\partial X}\right)^2\right]-\frac{3}{\varepsilon Pe_b}\frac{\chi}{h^2}+\frac{3\varepsilon h}{Pe_b^2k_s}\frac{\partial^2C}{\partial X^2}$$
$$-\frac{3\varepsilon Re}{80}\left[h\chi\left(M_1\frac{\partial^2\Gamma}{\partial X^2}+\frac{M_2}{h}\left\{\frac{\partial^2\phi}{\partial X^2}-\frac{2}{h}\frac{\partial h}{\partial X}\frac{\partial\phi}{\partial X}-\frac{\phi}{h}\frac{\partial^2h}{\partial X^2}+\frac{2\phi}{h^2}\left(\frac{\partial h}{\partial X}\right)^2\right\}\right)\right.$$
$$+\frac{\partial\chi}{\partial X}\left(M_1h\frac{\partial\Gamma}{\partial X}+M_2\left\{\frac{\partial\phi}{\partial X}-\frac{\phi}{h}\frac{\partial h}{\partial X}\right\}\right)$$
$$\left.+\chi\frac{\partial h}{\partial X}\left(M_1\frac{\partial\Gamma}{\partial X}+\frac{M_2}{h}\left\{\frac{\partial\phi}{\partial X}-\frac{\phi}{h}\frac{\partial h}{\partial X}\right\}\right)\right]. \tag{4.16}$$

$$\frac{\partial\Gamma}{\partial\tau}+\frac{\partial}{\partial X}\left[\frac{3}{2}\frac{q\Gamma}{h}\right]=\frac{\varepsilon}{Pe_s}\frac{\partial^2\Gamma}{\partial X^2}+\varepsilon Re\Gamma\frac{\partial h}{\partial X}\left[M_1\frac{\partial\Gamma}{\partial X}+\frac{M_2}{h}\left(\frac{\partial\phi}{\partial X}-\frac{\phi}{h}\frac{\partial h}{\partial X}\right)\right]+\frac{k_s}{\varepsilon}\frac{\chi}{h^2}$$
$$+\frac{\varepsilon Re}{4}\left[h\Gamma\left(M_1\frac{\partial^2\Gamma}{\partial X^2}+\frac{M_2}{h}\left\{\frac{\partial^2\phi}{\partial X^2}-\frac{2}{h}\frac{\partial h}{\partial X}\frac{\partial\phi}{\partial X}-\frac{\phi}{h}\frac{\partial^2h}{\partial X^2}+\frac{2\phi}{h^2}\left(\frac{\partial h}{\partial X}\right)^2\right\}\right)\right.$$
$$+\frac{\partial\Gamma}{\partial X}\left(M_1h\frac{\partial\Gamma}{\partial X}+M_2\left\{\frac{\partial\phi}{\partial X}-\frac{\phi}{h}\frac{\partial h}{\partial X}\right\}\right)$$
$$\left.+\Gamma\frac{\partial h}{\partial X}\left(M_1\frac{\partial\Gamma}{\partial X}+\frac{M_2}{h}\left\{\frac{\partial\phi}{\partial X}-\frac{\phi}{h}\frac{\partial h}{\partial X}\right\}\right)\right]. \tag{4.17}$$

As a check, we carried out a linear stability analysis on the above system and were able to reproduce the expression for the critical Reynolds number given by (3.14).

To numerically solve the system of (4.13)–(4.17) we first express these equations in the form

$$\frac{\partial h}{\partial\tau}+\frac{\partial q}{\partial X}=0,$$
$$\frac{\partial q}{\partial\tau}+\frac{\partial}{\partial X}\left[\frac{9}{7}\frac{q^2}{h}+\frac{5\cot\beta}{4Re}h^2+\frac{5M_1}{4}\Gamma+\frac{5M_2}{4}\frac{\phi}{h}\right]=S_1+Q_1,$$
$$\frac{\partial\phi}{\partial\tau}+\frac{\partial}{\partial X}\left[\frac{27}{20}\frac{q\phi}{h}\right]=S_2+Q_2,$$
$$\frac{\partial\chi}{\partial\tau}+\frac{\partial}{\partial X}\left[\frac{33}{40}\frac{q\chi}{h}\right]=S_3+Q_3,$$
$$\frac{\partial\Gamma}{\partial\tau}+\frac{\partial}{\partial X}\left[\frac{3}{2}\frac{q\Gamma}{h}\right]=S_4+Q_4,$$

where the gradient-free source terms S_1, S_2, S_3 are given by

$$S_1=\frac{5}{2\varepsilon Re}\left(h-\frac{q}{h^2}\right),\quad S_2=-\frac{3}{\varepsilon PrReh}\left[B(h+\phi)+\frac{\phi}{h}\right],\quad S_3=-\frac{3}{\varepsilon Pe_b}\frac{\chi}{h^2},\quad S_4=\frac{k_s}{\varepsilon}\frac{\chi}{h^2},$$

and Q_1, Q_2, Q_3, Q_4 can be easily determined from (4.14)–(4.17), respectively. To solve this system of equations the fractional-step splitting technique (Leveque 2002) was

implemented. We first solve

$$\frac{\partial h}{\partial \tau}+\frac{\partial q}{\partial X}=0,$$
$$\frac{\partial q}{\partial \tau}+\frac{\partial}{\partial X}\left[\frac{9}{7}\frac{q^2}{h}+\frac{5\cot\beta}{4Re}h^2+\frac{5M_1}{4}\Gamma+\frac{5M_2}{4}\frac{\phi}{h}\right]=S_1,$$
$$\frac{\partial \phi}{\partial \tau}+\frac{\partial}{\partial X}\left[\frac{27}{20}\frac{q\phi}{h}\right]=S_2,$$
$$\frac{\partial \chi}{\partial \tau}+\frac{\partial}{\partial X}\left[\frac{33}{40}\frac{q\chi}{h}\right]=S_3,$$
$$\frac{\partial \Gamma}{\partial \tau}+\frac{\partial}{\partial X}\left[\frac{3}{2}\frac{q\Gamma}{h}\right]=S_4,$$

over a time step $\Delta\tau$, and then solve

$$\frac{\partial q}{\partial \tau}=Q_1,\quad \frac{\partial \phi}{\partial \tau}=Q_2,\quad \frac{\partial \chi}{\partial \tau}=Q_3,\quad \frac{\partial \Gamma}{\partial \tau}=Q_4,$$

using the solution obtained from the first step as an initial condition for the second step. The second step then returns the solution for q, Γ, χ at the new time $\tau+\Delta\tau$.

The first step involves solving a nonlinear system of hyperbolic conservation laws which, when expressed in vector form, can be written compactly as

$$\frac{\partial \boldsymbol{U}}{\partial \tau}+\frac{\partial \boldsymbol{F}(\boldsymbol{U})}{\partial X}=\boldsymbol{B}(\boldsymbol{U}),$$

where

$$\boldsymbol{U}=\begin{bmatrix} h\\ q\\ \phi\\ \chi\\ \Gamma\end{bmatrix},\quad \boldsymbol{F}(\boldsymbol{U})=\begin{bmatrix} q\\ \dfrac{9q^2}{7h}+\dfrac{5\cot\beta h^2}{4Re}+\dfrac{5M_1\Gamma}{4}+\dfrac{5M_2\phi}{4h}\\ \dfrac{27q\phi}{20h}\\ \dfrac{33q\chi}{40h}\\ \dfrac{3q\Gamma}{2h}\end{bmatrix},\quad \boldsymbol{B}(\boldsymbol{U})=\begin{bmatrix} 0\\ S_1\\ S_2\\ S_3\\ S_4\end{bmatrix}.$$

While there are several schemes available to solve such a system, because of the complicated eigenstructure of the above system eigen-based methods will not be practical. Instead, MacCormack's method was adopted due to its relative simplicity. This is a conservative second-order accurate finite difference scheme which correctly captures discontinuities and converges to the physical weak solution of the problem. LeVeque & Yee (1990) extended MacCormack's method to include source terms via the explicit predictor–corrector scheme

$$\boldsymbol{U}_j^*=\boldsymbol{U}_j^n-\frac{\Delta\tau}{\Delta X}\left[\boldsymbol{F}(\boldsymbol{U}_{j+1}^n)-\boldsymbol{F}(\boldsymbol{U}_j^n)\right]+\Delta\tau\,\boldsymbol{B}(\boldsymbol{U}_j^n),$$
$$\boldsymbol{U}_j^{n+1}=\frac{1}{2}\left(\boldsymbol{U}_j^n+\boldsymbol{U}_j^*\right)-\frac{\Delta\tau}{2\Delta X}\left[\boldsymbol{F}(\boldsymbol{U}_j^*)-\boldsymbol{F}(\boldsymbol{U}_{j-1}^*)\right]+\frac{\Delta\tau}{2}\boldsymbol{B}(\boldsymbol{U}_j^*),$$

where the notation $\boldsymbol{U}_j^n \equiv \boldsymbol{U}(X_j, \tau_n)$ is utilized with ΔX denoting the uniform grid spacing and $\Delta\tau$ is the time step.

The second step reduces to solving a coupled system of generalized one-dimensional nonlinear diffusion equations with the understanding that h is determined from the first step and remains constant during the second step. For example, equation (4.16) for χ has the form

$$\frac{\partial \chi}{\partial \tau} = -\frac{3h}{Pe_b k_s}\frac{\partial C}{\partial \tau} - \frac{3q}{Pe_b k_s}\frac{\partial C}{\partial X} + \frac{3\varepsilon h}{Pe_b^2 k_s}\frac{\partial^2 C}{\partial X^2} + \frac{\varepsilon}{Pe_b}\frac{\partial^2 \chi}{\partial X^2} + \hat{Q}_1\frac{\partial \chi}{\partial X} + \hat{Q}_0\chi.$$

The functions $\hat{Q}_0$, $\hat{Q}_1$ do not depend on χ and can be easily obtained. However, C does depend on χ through the relation $\chi = h^2[\xi_s(1-\Gamma)C - \Gamma]$ which was used in the discretization process. This equation was discretized using the Crank–Nicolson scheme with central differencing applied to spatial derivatives. Also, periodicity conditions were imposed and the output from the first step was used as an initial condition. Solving the remaining equations in a similar manner leads to a nonlinear system of algebraic equations which was solved iteratively. A robust algorithm taking advantage of the structure and sparseness of the resulting linearized system was used to speed up the iterative process. It was found that convergence was reached quickly, typically in fewer than five iterations.

The evolution of the unsteady flow was computed by imposing a small perturbation on the constant equilibrium solutions h_E, q_E, ϕ_E, χ_E and Γ_E where

$$h_E = q_E = 1, \quad \phi_E = -\frac{B}{(1+B)}, \quad \chi_E = 0,$$

and $0 < \Gamma_E < 1$. By monitoring the growth of the disturbances as the perturbed solutions were marched in time we were able to estimate the onset of instability by carrying out numerous numerical experiments. In these experiments the computational domain was taken to have a length of $L = 20$, the grid spacing and time step were $\Delta X = 0.01$, $\Delta\tau = 0.001$, respectively, the parameter ε was set to 0.1 and periodicity conditions were imposed at the ends. Although the domain length is arbitrary, based on our numerical experiments it was judged that $L = 20$ was sufficiently large to trigger the long-wave instability. As numerical checks the volume of fluid and the total surfactant mass were computed at each time step and were observed to remain constant to within several decimal places.

By stepping the Reynolds number and noticing the first instance when the flow develops a permanent series of waves on the free surface we were able to bound the critical value of Re. We report here the findings of a case having the following parameter values: $\cot\beta = 1$, $\xi_s = 10$, $k_s = 1$, $\Gamma_E = 0.1$, $B = 0.1$, $M_1 = 1$, $M_2 = 2.07795$, $Pr = 7$ and $Pe_b = Pe_s = 700$. This particular configuration having moderate solubility was chosen because these values satisfy the condition given by (3.13) whereby the destabilizing thermocapillary effect exactly cancels the stabilizing solutocapillary effect. Hence, the critical Reynolds number for this set-up will be that of an isothermal pure liquid layer given by $Re_{crit} = 5\cot\beta/6 \approx 0.83$. From our numerical simulations we have determined that $0.8 < Re_{crit} < 0.9$; that is, for $Re = 0.8$ the disturbed flow settles to the equilibrium solution while for $Re = 0.9$ the disturbed flow becomes unstable. Thus, our nonlinear numerical simulation is in close agreement with the value predicted by linear theory. Next we present some unstable results for this configuration having $Re = 0.9$. Shown in figure 7 is the time evolution of the flow

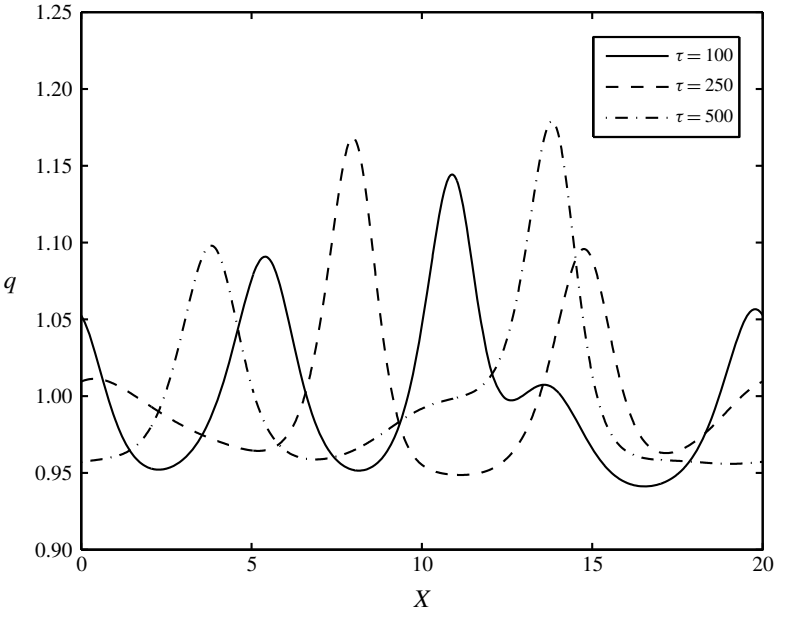

FIGURE 7. Time evolution of the flow rate.

rate, q. The diagram illustrates the transition in the development of waves as a result of the instability. We see that at $\tau = 100$ a series of four waves are present and with the passage of time the number of waves decreases to two at $\tau = 250$. Plotted in figure 8, on the other hand, is the time evolution of the surface surfactant concentration, Γ. This plot shows the formation of a prominent peak at $\tau = 500$. Lastly, illustrated in figure 9 is a snapshot of the fluid thickness, h, and the surface temperature, θ, at $\tau = 100$. Here we see that h produces a similar plot as q but with smaller amplitudes. Although there is little variation in θ due to the small value of B, we do notice that the surface temperature is lowest at the crests and largest at the troughs. This is consistent with the prescribed temperature profile which decreases linearly from the incline to the free surface. Thus, at the crests the temperature drops the most while at the troughs it drops the least.

Lastly, we present some results which include an additional capillary term. In our model a capillary term was neglected because it is $O(\varepsilon^3)$. However, for strong surface tension having $We = O(1/\varepsilon)$ this capillary term will make an appearance. We entertained this case by setting $We = We_1/\varepsilon$ and added the following to the right-hand side of (4.14)

$$\frac{5\varepsilon We_1}{6} h \frac{\partial^3 h}{\partial x^3}.$$

Plotted in figures 10–12 are results obtained for the parameter values: $M_1 = M_2 = B = \cot\beta = k_s = 1$, $\xi_s = 10$, $\Gamma_E = 0.05$, $Pe_b = Pe_s = 700$, $Pr = 7$, $We_1 = 5$ and $Re = 1.5$. Figure 10 shows a wave pattern consisting of two waves accompanied by small amplitude capillary oscillations at their fronts. We also observed that on a shorter computational domain having $L = 5$ a single-hump solitary-type wave emerged. Figure 11 illustrates the surface surfactant concentration at various times while figure 12 portrays the fluid thickness and surface temperature at $\tau = 500$.

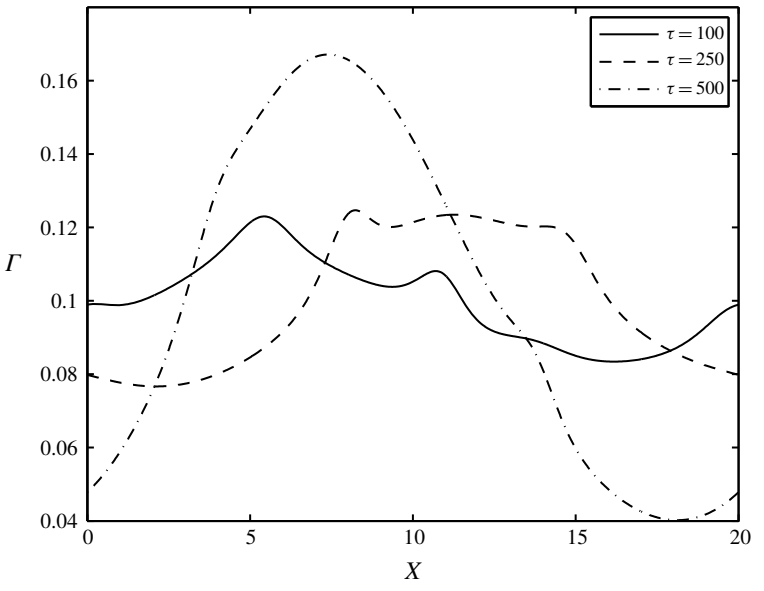

FIGURE 8. Time evolution of the surface surfactant concentration.

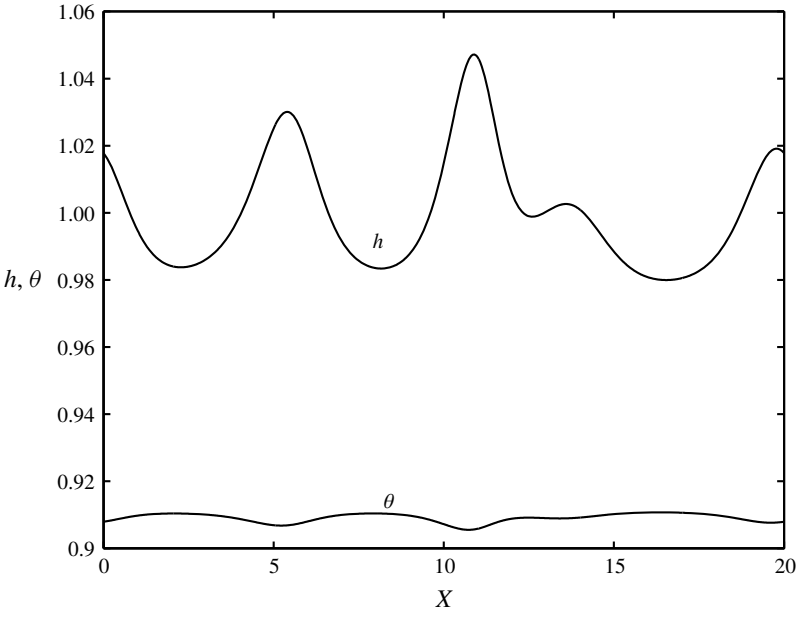

FIGURE 9. The fluid thickness and surface temperature at $\tau = 100$.

5. Concluding remarks

We reported on the stability of a gravity-driven flow of a surfactant-laden liquid layer down a heated incline in this study. The interaction of solutal and thermal effects was thoroughly investigated. A linear stability analysis of the steady flow of a film with uniform thickness was conducted which led to an eigenvalue problem governing the evolution of infinitesimal perturbations. An asymptotic analysis yielded a formula

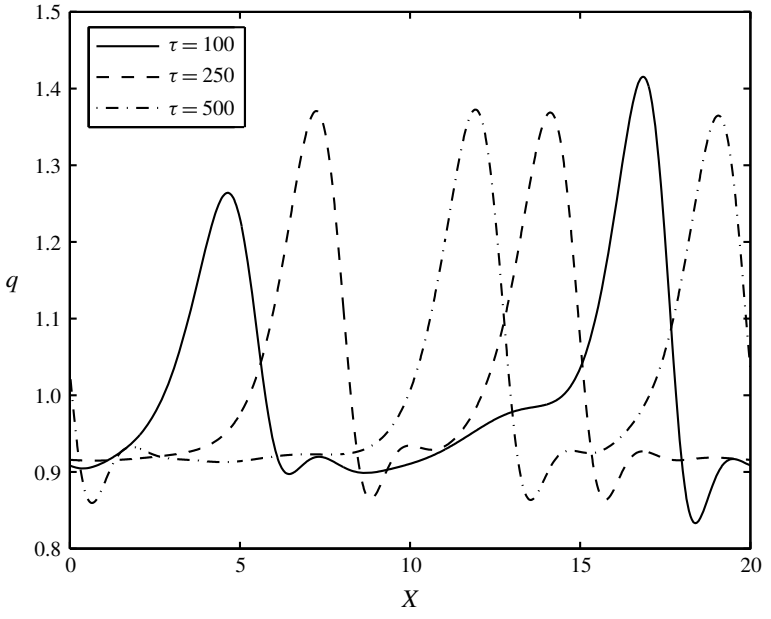

FIGURE 10. Time evolution of the flow rate.

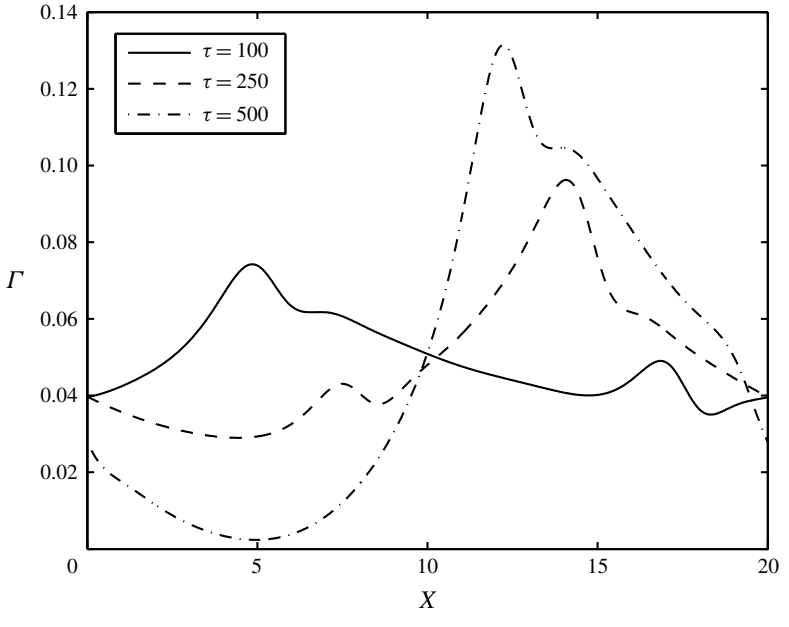

FIGURE 11. Time evolution of the surface surfactant concentration.

for the neutral stability pertaining to perturbations having small wavenumbers which is in full agreement with previous results for special cases. These results were also verified by numerical solutions of the eigenvalue problem for arbitrary wavenumbers. The key findings include the fact that adding a surfactant enhances inertial instability if thermocapillarity is sufficiently strong, however the strict Marangoni instability mode is stabilized for very small Reynolds numbers.

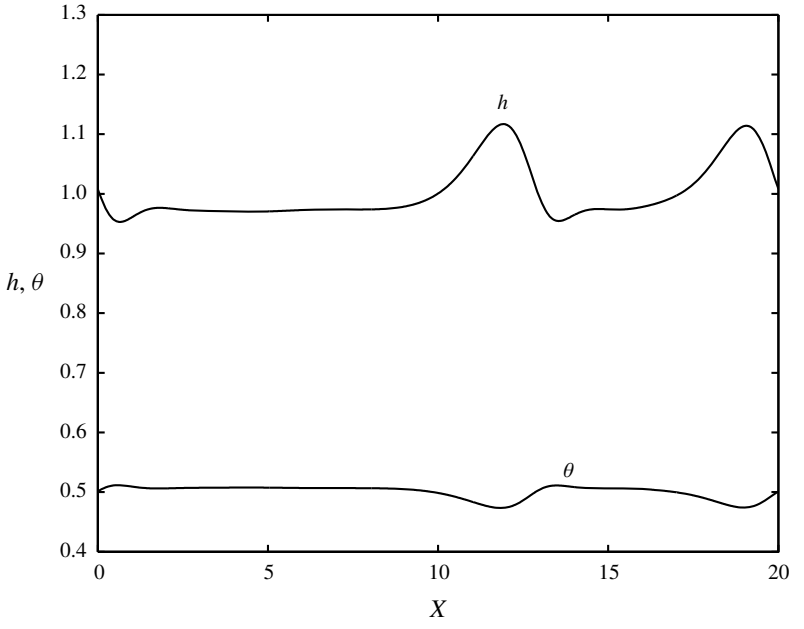

FIGURE 12. The fluid thickness and surface temperature at $\tau = 500$.

In addition, nonlinear effects were also investigated using a second-order weighted residual model. The nonlinear simulations were in good agreement with the predictions made by the Orr–Sommerfeld equations for the onset of instability. For unstable flows the simulations revealed the formation of permanent waves propagating along the free surface. For large Weber numbers these waves have small amplitude capillary oscillations formed at their fronts.

Acknowledgements

Financial support for this research was provided by the Natural Sciences and Engineering Research Council of Canada and the Faculty of Mathematics at the University of Waterloo.

Appendix A. Linear stability in the limit of a non-deformable interface

We consider the limit of a non-deformable interface of constant height $h = 1$. In this case, the momentum balance, heat balance and governing equations for the surfactant concentrations are decoupled. The perturbations of surfactant concentrations within the bulk and adsorbed at the free surface, denoted by $\tilde{c}$ and $\tilde{\Gamma}$ respectively, then satisfy

$$Pe_b \frac{\partial \tilde{c}}{\partial t} = \frac{\partial^2 \tilde{c}}{\partial z^2}, \tag{A 1}$$

$$\frac{\partial \tilde{\Gamma}}{\partial t} = k_s \left[\xi_s (1 - \Gamma_E) \tilde{c} - \frac{\tilde{\Gamma}}{(1 - \Gamma_E)} \right], \tag{A 2}$$

subject to the boundary conditions

$$\frac{\partial \tilde{c}}{\partial z} = -Pe_b \frac{\partial \tilde{\Gamma}}{\partial t} \quad \text{at } z = 1, \tag{A 3}$$

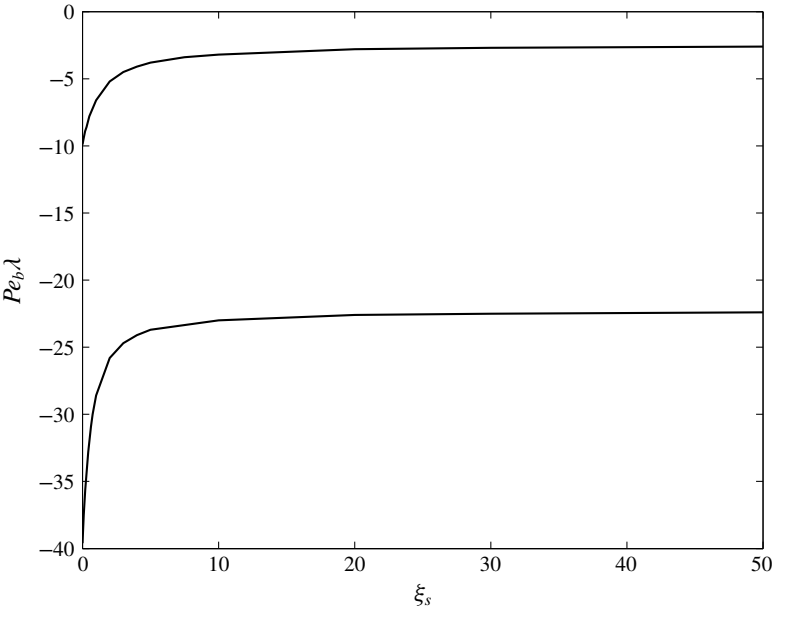

FIGURE 13. The first two eigenvalues, $Pe_b\lambda$, as a function of ξ_s with $Pe_b = 700$, $\Gamma_E = 0.5$ and $k_s = 1$.

$$\frac{\partial \tilde{c}}{\partial z} = 0 \quad \text{at } z = 0. \tag{A 4}$$

Assuming solutions of the form

$$\tilde{c} = \mathrm{e}^{\lambda t}\cos(lz), \quad \tilde{\Gamma} = \mathrm{e}^{\lambda t}\hat{\Gamma}, \tag{A 5}$$

where λ and l denote the growth rate and wavenumber, respectively, and substituting into (A 1)–(A 4) yields the dispersion relation

$$l^2 \sin l - Pe_b k_s \left[\xi_s(1-\Gamma_E) l \cos l + \frac{\sin l}{(1-\Gamma_E)}\right] = 0, \tag{A 6}$$

with

$$\lambda = -\frac{l^2}{Pe_b} \quad \text{and} \quad \hat{\Gamma} = -\frac{\sin l}{l}.$$

In the insoluble limit $\xi_s \gg 1$, equation (A 6) reduces to $\cos l = 0$, with $l = \pi/2 + n\pi$. Similarly, in the limit $\xi_s \to 0$, $l = \pi + n\pi$. All of these solutions correspond to real and negative eigenvalues, thus these eigenmodes are relaxation eigenmodes associated with the dissipation of kinetic energy by viscosity. Figure 13 shows the two first eigenvalues for the parameter values $Pe_b = 700$, $\Gamma_E = 0.5$ and $k_s = 1$. We observe that in the insoluble limit $Pe_b\lambda \to -\pi^2/4 \approx -2.5$ for the first eigenvalue and it is approached rather quickly as ξ_s increases from zero.

As discussed in Ruyer-Quil *et al.* (2014), following the centre manifold approach introduced by Roberts (1995), a successful modelling should approach the eigenmode associated with the displacement of the free surface (kinematic neutral eigenmode)

and the viscous relaxation modes. An appropriate choice for the test functions in our weighted residual procedure should consist of linear combinations of the viscous eigenmodes solutions of (A 5) and (A 6). Hence, l is obtained implicitly and not explicitly. Also, sinusoidal functions introduce non-fractional numbers which unnecessarily complicate the expressions for the coefficients in the model.

Since the insoluble limit is achieved rather quickly as ξ_s increases, we assume l to be close to $\pi/2$. Here, we chose a trade-off between complexity and accuracy, namely $1 - z^2$ which is a simple polynomial approximation to $\cos(\pi z/2)$. The relaxation eigenvalue λ is then approached by $-3/Pe_b$, which is the coefficient of the damping term $-(3/Pe_b)\chi/h^2$ in our evolution equation for χ given by (4.16). Figure 13 shows that this coefficient is an acceptable approximation to the first relaxation eigenvalue for a wide range of ξ_s values.

REFERENCES

AKSEL, N. & SCHÖRNER, M. 2018 Films over topography: from creeping flow to linear stability, theory, and experiments, a review. *Acta Mech.* **229**, 1453–1482.

BENJAMIN, T. B. 1957 Wave formation in laminar flow down an inclined plane. *J. Fluid Mech.* **2**, 554–574.

BENJAMIN, T. B. 1964 Effects of surface contamination on wave formation in falling liquid films. *Arch. Mech. Stos.* **16**, 615–626.

BLYTH, M. G. & POZRIKIDIS, C. 2004 Effect of surfactant on the stability of film flow down an inclined plane. *J. Fluid Mech.* **521**, 241–250.

D'ALESSIO, S. J. D., PASCAL, J. P., JASMINE, H. A. & OGDEN, K. A. 2010 Film flow over heated wavy inclined surfaces. *J. Fluid Mech.* **665**, 418–456.

D'ALESSIO, S. J. D. & PASCAL, J. P. 2016 Thermosolutal Marangoni effects on the inclined flow of a binary liquid with variable density. II. Nonlinear analysis and simulations. *Phys. Rev. Fluids* **1**, 083604.

D'ALESSIO, S. J. D., PASCAL, J. P. & JASMINE, H. A. 2009 Instability in gravity-driven flow over uneven surfaces. *Phys. Fluids* **21**, 062105.

ELLABAN, E., PASCAL, J. P. & D'ALESSIO, S. J. D. 2017 Instability of a binary liquid film flowing down a slippery heated plate. *Phys. Fluids* **29**, 092105.

EMMERT, R. E. & PIGFORD, R. 1954 A study of gas absorption in falling liquid films. *Chem. Engng Prog.* **50**, 87–93.

FLORYAN, J. M., DAVIS, S. H. & KELLY, R. E. 1987 Instabilities of a liquid film flowing down a slightly inclined plane. *Phys. Fluids* **30**, 983–989.

GEORGANTAKI, A., VLACHOGIANNIS, M. & BONTOZOGLOU, V. 2016 Measurements of the stabilisation of liquid film flow by the soluble surfactant sodium dodecyl sulfate (SDS). *Intl J. Multiphase Flow* **86**, 28–34.

GOUSSIS, D. A. & KELLY, R. E. 1991 Surface wave and thermocapillary instabilities in a liquid film flow. *J. Fluid Mech.* **223**, 25–45.

JI, W. & SETTERWALL, F. 1995 Effect of heat transfer additives on the instabilities of an absorbing falling film. *Chem. Engng Sci.* **50**, 3077–3097.

JI, W. & SETTERWALL, F. 1994 On the instabilities of vertical falling liquid films in the presence of surface-active solute. *J. Fluid Mech.* **278**, 297–323.

KALLIADASIS, S., DEMEKHIN, E. A., RUYER-QUIL, C. & VELARDE, M. G. 2003*a* Thermocapillary instability and wave formation on a film falling down a uniformly heated plane. *J. Fluid Mech.* **492**, 303–338.

KALLIADASIS, S., KIYASHKO, A. & DEMEKHIN, E. A. 2003*b* Marangoni instability of a thin liquid film heated from below by a local heat source. *J. Fluid Mech.* **475**, 377–408.

KALLIADASIS, S., DEMEKHIN, E. A., RUYER-QUIL, C. & VELARDE, M. G. 2012 *Falling Liquid Films*. Springer.

KAPITZA, P. L. & KAPITZA, S. P. 1949 Wave flow of thin layers of a viscous fluid. Part III. Experimental study of undulatory flow conditions. *Soc. Phys. J. Exp. Theor. Phys.* **19**, 105–120.

KARAPETSAS, G. & BONTOZOGLOU, V. 2013 The primary instability of falling films in the presence of soluble surfactants. *J. Fluid Mech.* **729**, 123–150.

KARAPETSAS, G. & BONTOZOGLOU, V. 2014 The role of surfactants on the mechanism of long-wave instability in liquid film flows. *J. Fluid Mech.* **741**, 139–155.

LEVEQUE, R. J. 2002 *Finite Volume Methods for Hyperbolic Problems*. Cambridge University Press.

LEVEQUE, R. J. & YEE, H. C. 1990 A study of numerical methods for hyperbolic conservation laws with stiff source terms. *J. Comput. Phys.* **86**, 187–210.

NEPOMNYASHCHY, A. A., VELARDE, M. G. & COLINET, P. 2002 *Interfacial Phenomena and Convection*. CRC.

OGDEN, K. A., D'ALESSIO, S. J. D. & PASCAL, J. P. 2011 Gravity-driven flow over heated, porous, wavy surfaces. *Phys. Fluids* **23**, 122102.

PASCAL, J. P., D'ALESSIO, S. J. D. & ELLABAN, E. 2019 Stability of inclined flow of a liquid film with soluble surfactants and variable mass density. *Phys. Rev. Fluids* **4**, 054004.

PASCAL, J. P. & D'ALESSIO, S. J. D. 2016 Thermosolutal Marangoni effects on the inclined flow of a binary liquid with variable density. I. Linear stability analysis. *Phys. Rev. Fluids* **1**, 083603.

PASCAL, J. P. & D'ALESSIO, S. J. D. 2010 Instability in gravity-driven flow over uneven permeable surfaces. *Intl J. Multiphase Flow* **36**, 449–459.

PASCAL, J. P., D'ALESSIO, S. J. D. & HASAN, M. 2018 Instability of gravity-driven flow of a heated power-law fluid with temperature dependent consistency. *AIP Adv.* **8**, 105215.

PEARSON, J. 1958 On convection cells induced by surface tension. *J. Fluid Mech.* **4**, 489–500.

PEREIRA, A., TREVELYAN, P. M. J., THIELE, U. & KALLIADASIS, S. 2007 Dynamics of a horizontal thin liquid film in the presence of reactive surfactants. *Phys. Fluids* **19**, 112102.

PEREIRA, A. & KALLIADASIS, S. 2008 Dynamics of a falling film with solutal Marangoni effect. *Phys. Rev.* E **78**, 036312.

PEREIRA, A. & KALLIADASIS, S. 2011 On the transport equation for an interfacial quantity. *Eur. Phys. J. Appl. Phys.* **44** (2), 211–214.

ROBERTS, A. J. 1995 Low-dimensional models of thin film fluid dynamics. *Phys. Lett.* A **212**, 63–71.

RUYER-QUIL, C., SCHEID, B., KALLIADASIS, S., VELARDE, M. G. & ZEYTOUNIAN, R. KH. 2005 Thermocapillary long waves in a liquid film flow. Part 1. Low-dimensional formulation. *J. Fluid Mech.* **538**, 199–222.

RUYER-QUIL, C. & MANNEVILLE, P. 2000 Improved modeling of flows down inclined planes. *Eur. Phys. J.* B **15**, 357–369.

RUYER-QUIL, C. & MANNEVILLE, P. 2002 Further accuracy and convergence results on the modeling of flows down inclined planes by weighted-residual approximations. *Phys. Fluids* **14**, 170–183.

RUYER-QUIL, C., KOFMAN, N., CHASSEUR, D. & MERGUI, S. 2014 Dynamics of falling films. *Eur. Phys. J.* E **37** (4), 1–17.

SCHEID, B., RUYER-QUIL, C., KALLIADASIS, S., VELARDE, M. G. & ZEYTOUNIAN, R. KH. 2005 Thermocapillary long waves in a liquid film flow. Part 2. Linear stability and nonlinear waves. *J. Fluid Mech.* **538**, 223–244.

SHELUDKO, A. 1967 Thin liquid films. *Adv. Colloid Interface Sci.* **1**, 391–464.

SPURK, J. H. & AKSEL, N. 2008 *Fluid Mechanics*, 2nd edn. Springer.

SRIVASTAVA, A. & TIWARI, N. 2018 Effect of an insoluble surfactant on the dynamics of a thin liquid film flowing over a non-uniformly heated substrate. *Eur. Phys. J.* E **41**, 1–12.

STERNLING, C. V. & SCRIVEN, L. E. 1959 Interfacial turbulence: hydrodynamic stability and the Marangoni effect. *AIChE J.* **5**, 514–523.

STIRBA, C. & HURT, D. 1955 Turbulence in falling liquid films. *AIChE J.* **1**, 178–184.

TAILBY, S. & PORTALSKI, S. 1961 The optimum concentration of surface active agents for the suppression of ripples. *Trans. Inst. Chem. Engrs* **39**, 328–336.

TREFETHEN, L. N. 2000 *Spectral Methods in Matlab*. SIAM.

TREVELYAN, P. M. J., SCHEID, B., RUYER-QUIL, C. & KALLIADASIS, S. 2007 Heated falling films. *J. Fluid Mech.* **592**, 295–334.

VEREMIEIEV, S. & WACKS, D. H. 2019 Modelling gravity-driven film flow on inclined corrugated substrate using a high fidelity weighted residual integral boundary-layer method. *Phys. Fluids* **31**, 022101.

WEI, H. 2005 Effect of surfactant on the long-wave instability of a shear-imposed liquid flow down an inclined plane. *Phys. Fluids* **17**, 012103.

WHITAKER, S. 1964 Effect of surface active agents on the stability of falling liquid films. *Ind. Engng Chem. Fundam.* **3**, 132–142.

YIH, C.-S. 1963 Stability of liquid flow down an inclined plane. *Phys. Fluids* **6**, 321–334.